Open access • Journal Article • DOI:10.1029/96JE02036

Vertical distribution of Titan's atmospheric neutral constituents — Source link

Luisa Lara, Emmanuel Lellouch, J. J. Lopez-Moreno, Rafael Rodrigo

Published on: 25 Oct 1996 - Journal of Geophysical Research (John Wiley & Sons, Ltd)

Topics: Mixing ratio, Reaction rate and Methane

JOURNAL OF GEOPHYSICAL RESEARCH, VOL. 101, NO. E10, PAGES 23,261–23,283, OCTOBER 25, 1996

Vertical distribution of Titan's atmospheric neutral constituents

L. M. Lara

Département de Recherches Spatiales Observatoire de Paris–Meudon, Meudon, France
Instituto de Astrofísica de Andalucía, Consejo Superior de Investigaciones Scientificas, Granada, Spain

E. Lellouch

Département de Recherches Spatiales Observatoire de Paris–Meudon, Meudon, France

J. J. López-Moreno and R. Rodrigo

Instituto de Astrofísica de Andalucía, CSIC, Granada, Spain

Abstract. The vertical distribution of Titan's neutral atmosphere compounds is calculated from a new photochemical model extending from 40 to 1432 km. This model makes use of many updated reaction rates, and of the new scheme for methane photolysis proposed by *Mordaunt et al.* [1993]. The model also includes a realistic treatment of the dissociation of N_2, of the deposition of water in the atmosphere from meteoritic ablation, and of condensation processes. The sensitivity of the results to the eddy diffusion coefficient profile is investigated. Fitting the methane thermospheric profile and the stratospheric abundance of the major hydrocarbons requires a methane stratospheric mixing ratio of 1.5–2% rather than 3%. Fitting the HCN stratospheric profile requires an eddy diffusion coefficient at 100–300 km that is 5–20 times larger than that necessary for the hydrocarbons. Most species are reasonably well reproduced, with the exception of CH_3C_2H and HC_3N. The formation of CH_3CN may involve the reaction of CN with either CH_4 or (preferably) C_2H_6. The observed CO_2 profile can be modeled by assuming an external source of water of $\sim 6 \times 10^6$ cm^{-2} s^{-1}. For a nominal CO mixing ratio of 5×10^{-5}, the chemical loss of CO exceeds its production by ~15%, and equilibrium is achieved for CO = 1×10^{-5}.

1. Introduction

Titan, a satellite with massive atmosphere, has attracted considerable attention in the past two decades. Methane and other hydrocarbons dominate the infrared spectrum, while the major gas is N_2 and trace amounts of oxygen compounds and nitriles are present. The stratosphere and mesosphere contain optically thick layers of dark orange haze particles. These aerosols are thought to be the end product of methane and nitrogen photochemistry and to either accumulate on a solid surface or dissolve in liquid methane/ethane ocean or lakes [*Lunine et al.*, 1983; *Raulin*, 1987; *Toon et al.*, 1988; *Dubouloz et al.*, 1989].

Pre-Voyager photochemical models [*Strobel*, 1974; *Allen et al.*, 1980] were restricted to hydrocarbons, the only species known for sure at that time, although the possibility of a nitrogen-rich atmosphere had also been considered [*Lewis*, 1971; *Hunten*, 1978; *Atreya et al.*, 1978]. In particular, *Allen et al.* [1980] investigated the formation of aerosols and their variations over a solar cycle. Such variations were linked to the existence of a positive feedback mechanism in the production of polyynes ($C_{2n}H_2$). The modeled number densities of major hydrocarbon species were in agreement with the then available measurements but now appear to differ from post-Voyager determinations by more than 1 order of magnitude.

Post-Voyager chemical models of Titan's atmosphere can be classified in two categories: (1) photochemical models, describing gas phase chemical pathways and aiming at reproducing the atmospheric gaseous composition and (2) microphysical models, which are primarily concerned with the growth rates and the size and number density versus altitude distribution of the stratospheric aerosols. The intermediate step, i.e., the formation of small organic nuclei from the condensation and polymerization of complex hydrocarbons and nitriles, remains essentially unmodeled, although clues on the mechanisms at work may be inferred from laboratory simulations [e.g., *Thompson and Sagan*, 1991]. While many microphysical models have been developed [*Podolak and Podolak*, 1980; *Rages and Pollack*, 1980, 1983; *Rages et al.*, 1983; *Podolak et al.*, 1984; *Frère et al.*, 1990; *Cabane et al.*, 1992; *Toon et al.*, 1992], providing a fairly detailed picture of the aerosol vertical distribution, modern photochemical models are, in comparison, relatively lacking, perhaps owing to the complexity of a chemistry simultaneously involving carbon, nitrogen, and oxygen compounds. A first attempt to model the chemistry in the presence of dominant N_2 gas was performed by *Strobel* [1982]. He found that the major effect of N_2 on the hydrocarbon chemistry was the rapid quenching of some molecular or atomic excited states. For example, singlet excited methylene ($^1CH_2$) is deactivated to its ground state and becomes a source of acetylene at high altitudes. Likewise, N_2 deactivates $O(^1D)$ to its ground state, $O(^3P)$, which controls the oxidation processes in the atmosphere (e.g., the production of CO with release of atomic and molecular hydrogen from reaction with CH_2 [*Samuelson et al.*, 1983]). In addition, the presence of N_2 allows the formation of nitriles from nitrogen atoms and ions. However, while key chemical pathways were identified, no profiles for the individ-

Paper number 96JE02036.
0148-0227/96/96JE-02036$09.00

ual species were derived and, consequently, no comparison with observational data was possible.

The first detailed photochemical model since Voyager was developed by *Yung et al.* [1984] (and updated by *Yung* [1987]). This work made use of a very complete set of chemical reactions, based on the compilation of the earlier studies by *Strobel* [1974, 1982] and *Allen et al.* [1980], and adding the photochemistry of oxygen compounds in a mildly reducing atmosphere (investigated by *Pinto et al.* [1980]), as well as new chemical reactions, mainly those forming long-chain hydrocarbons or polyynes. Vertical profiles for all the constituents observed in Titan's atmosphere were derived, and average mixing ratios were compared to early analyses of Voyager infrared observations [*Hanel et al.*, 1981; *Maguire et al.*, 1981; *Kunde et al.*, 1981; *Samuelson et al.*, 1983]. Implications of the model for the composition of the troposphere, the origin and evolution of the atmosphere, and the geochemistry were also assessed.

Despite the qualitative and quantitative importance of this work, there are at least two reasons to reconsider Titan's photochemical models today. First, several new observational constraints have become available. The Voyager infrared imaging spectrometer (IRIS) spectra at the equator have been more fully exploited, resulting in improved determinations of the mixing ratios, in well-understood altitude ranges [*Coustenis et al.*, 1989]. Vertical information is also available for some minor constituents observed in the north polar region [*Coustenis et al.*, 1991]. A reanalysis of the Voyager ultraviolet spectrometer (UVS) data has also been performed, resulting in a new vertical profile for CH_4 [*Strobel et al.*, 1992]. In addition, following a very accurate prediction by *Paubert et al.* [1984], ground-based observations at millimeter wavelengths have resulted in the detection of CO, HCN, HC_3N, and CH_3CN and in the measurement of their vertical profiles. Second, many relevant reaction rates have been recently (re)measured or reestimated, and a new scheme of the methane photolysis at Lyα has been proposed [*Mordaunt et al.*, 1993]. On the basis of this new information, we and *Toublanc et al.* [1995] were separately prompted to reexamine Titan's photochemistry. In addition to the above changes in the chemistry, the new ingredients in the Toublanc et al. study, compared to that of *Yung et al.* [1984], were (1) a Monte-Carlo treatment of the transfer of the solar radiation in the atmosphere, including scattering by the aerosols and (2) the choice of another eddy diffusion coefficient, adjusted to match the vertical distribution of HCN, as inferred by *Tanguy et al.* [1990].

We here present a one-dimensional, steady state model of Titan's low-latitude atmosphere, in the 40- to 1432-km range, valid for moderate solar activity. When available, the model incorporates updated laboratory kinetics data (see section 3.2) and photoabsorption cross sections (see section 3.1). We use a simple description (i.e., no scattering) of the light propagation in Titan's atmosphere. The new aspects of our model are (1) an improved treatment of condensation processes (see section 3.5), (2) the inclusion of dissociation profiles of molecular nitrogen (i.e., of production profiles of $N(^4S)$ and $N(^2D)$ by EUV and galactic cosmic rays (see section 3.4)), and (3) the inclusion of physically based water ablation profiles as a source of oxygen (see section 3.3). In the *Yung et al.* [1984] model the sources of nitrogen and oxygen were described by a specified influx of H_2O, $N(^4S)$, and $N(^2D)$ at the top of the model. Toublanc et al. improved the description for nitrogen by modeling the dissociation of N_2 by EUV radiation, but they retained the same approach as Yung et al. for oxygen. In addition, we have performed a sensitivity study of the vertical distributions to the eddy diffusion profile.

2. Model General Description

For every atmospheric constituent i, we solve the usual continuity equations in steady state conditions and in spherical geometry:

$$P_i - n_i l_i = \frac{1}{r^2}\frac{\partial}{\partial r}(r^2\Phi_i) \tag{1}$$

where Φ_i, the vertical flux, can be expressed as

$$\Phi_i = -n_i D_i\left(\frac{1}{n_i}\frac{\partial n_i}{\partial r} + \frac{1+\alpha_i}{T}\frac{\partial T}{\partial r} + \frac{1}{H_i}\right) - n_i K\left(\frac{1}{n_i}\frac{\partial n_i}{\partial r} + \frac{1}{T}\frac{\partial T}{\partial r} + \frac{1}{H}\right) \tag{2}$$

where n_i is the number density, P_i is the volumic production rate, l_i is the volumic specific loss rate, r is the radius ($r = R_0 + z$, where R_0 is Titan's radius), D_i is the molecular diffusion coefficient, T is temperature, H_i and H are the individual and atmospheric scale heights, respectively, K is the eddy diffusion coefficient, and α_i is the thermal diffusion coefficient.

For the temperature and N_2 number density profiles, we used the recommended model of *Yelle et al.* [1996]. This profile, derived from the physically based profiles of *Yelle* [1991], is very similar to the earlier nominal profiles of *Lellouch and Hunten* [1987] and *Lellouch et al.* [1989] below 200 km, but significantly different above this altitude. The lower boundary condition is taken at 40 km and the upper boundary at 1432 km, and the integration step in altitude is 6 km, which provides approximately 5 and 15 vertical steps per scale height in the stratosphere and mesosphere, respectively.

The species included in this model are N_2 (molecular nitrogen), CH_4 (methane), C_2H_2 (acetylene), C_2H_4 (ethylene), C_2H_6 (ethane), CH_3C_2H (methyl acetylene), C_3H_8 (propane), C_4H_2 (diacetylene), H, H_2, HCN (hydrogen cyanide), CH_3CN (acetonitrile), HC_3N (cyanoacetylene), C_2N_2 (cyanogen), C_4N_2 (dicyanogen), CO (carbon monoxide), CO_2 (carbon dioxide), H_2O (water vapor), $O(^3P)$, $O(^1D)$, $N(^2D)$, $N(^4S)$ and the radicals CH_3 (methyl), CH, $^1CH_2$, $^3CH_2$, C_2, C_2H, C_2H_3, C_2H_5, C_3H_2, C_3H_3, C_3H_5, C_4H, $C_4H_2^*$, C_4H_3, CN, C_3N, H_2C_3N, HC_2N_2, H_2CN, NH, CHCN, HCO, and OH.

An extensive study of the loss and production processes for each species indicates that the oxygen and nitrogen chemistry is very dependent on the distribution of hydrocarbon compounds, but that in contrast, it impacts only as a minor perturbation on the hydrocarbon chemistry, allowing a separation of the species in two classes. Because the number of oxygen compounds in our model is small, they were grouped with the hydrocarbons with no significant increase of the complexity. Thus we divided the species into two families: (1) hydrocarbons + oxygen compounds and (2) nitrogen compounds.

The vertical distributions of the hydrocarbon and oxygen compounds were calculated without including the nitrogen species (except N_2, of course). These distributions were then used to calculate the concentrations of the nitrogen compounds. This approach is similar to that adopted by *Yung et al.* [1984], and also by *Lellouch et al.* [1994] in their model of the HCN chemistry on Neptune. In each group, the continuity

equations were solved for all the long-lived constituents, using a Crank-Nicholson scheme [*Rodrigo et al.*, 1990]. In order to save computation time, the distributions of the short-lived species, which are in photochemical equilibrium throughout the atmosphere, were simply computed by dividing level by level their chemical production by their specific loss. In order to determine what species were short-lived, we used as an initial guess the distributions found by *Yung et al.* [1984] and compared their chemical lifetime to the transport time constant at various levels in the atmosphere. A posteriori checks were performed using the distributions found in this model. These short-lived species are $O(^1D)$, $N(^2D)$, and the radicals CH, $^1CH_2$, $^3CH_2$, C_2, C_2H, C_2H_3, C_2H_5, C_4H, $C_4H_2^*$, C_4H_3, CN, C_3N, H_2C_3N, HC_2N_2, H_2CN, NH, CHCN, and OH.

Lower and upper boundary conditions have been chosen according to the physical processes taking place at the corresponding levels. At the lower boundary (40 km), the mixing ratio of the condensible species (C_2H_2, C_2H_6, CH_3C_2H, C_3H_8, C_4H_2, HCN, CH_3CN, HC_3N, C_2N_2, C_4N_2, CO_2, and H_2O) was assumed to be determined by the saturation law (see Table 3). For the noncondensible, long-lived compounds (CH_4, H_2, and CO), we took their mixing ratios at the lower boundary from their observed values in the lower stratosphere. We note that the stratospheric methane mixing ratio is still not well constrained. *Lellouch et al.* [1989], assuming no supersaturation of CH_4, indicated that any value between 0.5% and 3.4% can satisfy the Voyager infrared and radiooccultation measurements. From a recent reanalysis of the IRIS spectra, *Courtin et al.* [1995] have suggested a possible supersaturation of CH_4 in the troposphere, which widens even more (up to 4.4%) the range of allowed CH_4. We started with a stratospheric CH_4 mixing ratio of 3%, which is the preferred value of *Strobel et al.* [1992] and of *Yelle et al.* [1996], but we also tested different values. For C_2H_4, we assumed a mixing ratio of 1.5×10^{-7} at 40 km, which is very close to the saturation value. Finally, although transport is important for determining the profiles of H, CH_3, HCO, $O(^3P)$, and $N(^4S)$, these species appear to be in local photochemical equilibrium in the lower atmosphere, allowing us to calculate their mixing ratio at the lower boundary. At the upper boundary, zero flux was assumed for all species, except for H, H_2, $O(^3P)$, and $N(^4S)$, which were allowed to escape with velocities given by Jeans' thermal escape mechanism. Convergence in each family was reached when successive iterations yielded solutions differing by less than 1 part in 10^4.

3. Photochemistry

Photochemistry in Titan's stratosphere is initiated by the absorption of solar radiation and the dissociation of atmospheric molecules. Gas phase chemical reactions and vertical transport primarily determine the distribution of minor species. In addition, the low temperatures in the lower stratosphere ($z \leq 100$ km) result in a strong condensation sink for a number of species. In what follows, we review our treatment of the photolysis, of the atmospheric chemistry (with particular attention about the source of water and the nitrogen dissociation), and of the condensation processes.

3.1. Photolysis

We use a simple classical treatment of the photolysis processes, similar to that presented by *Yung et al.* [1984]. Photodissociation reactions with their quantum yields are listed in Table 1. Photodissociation coefficients are calculated according to

$$J_i(z) = \int_{\lambda_1}^{\lambda_2} \sigma_{i,\lambda} \Phi(z, \lambda)\, d\lambda \tag{3}$$

where $\Phi(z, \lambda)$ is the solar flux at altitude z and wavelength λ. $\Phi(z, \lambda)$ can be expressed as a function of the diurnally averaged unattenuated solar flux at the top of the atmosphere, $\Phi_\infty(\lambda)$, of the molecular concentrations $n_i(z)$ and of the absorption cross sections $\sigma_{i,\lambda}$, according to

$$\Phi(z, \lambda) = \Phi_\infty(\lambda) \exp\left[-\int_{z'=z}^{+\infty} \left(\sum_i \sigma_{i,\lambda} n_i(z') \alpha_z \right) dz' \right] \tag{4}$$

where α_z is the Chapman function of the solar zenith angle. We use a solar zenith angle of 30°, representative of mean daytime equatorial conditions for optically thick absorption.

Unattenuated solar fluxes were taken from *Mount and Rottman* [1983], suitable for moderate solar activity, and rescaled to the Sun-Titan distance. Photodissociation coefficients for N_2 were calculated by integration of (3) from 8 to 80 nm. For other species the total wavelength range extended from 115 to 278 nm (radiation at Lyman α being considered separately) and was divided into spectral intervals of 0.2 nm, given the sharp variations with wavelength of the cross sections of some species. Absorption cross sections for methane (at 115–145 nm) and ethane were taken from *Atreya* [1986]; for acetylene, we used values from *Nakayama and Watanabe* [1964] and *Okabe* [1981, 1983]; ethylene data were taken from *Zelikoff and Watanabe* [1953]. For diacetylene, we used values from *Okabe* [1981] and *Glicker and Okabe* [1987]; for methyl acetylene, we used *Nakayama and Watanabe* [1964]. Propane data were taken from *Koch and Skibowsky* [1971], and hydrogen cyanide absorption cross sections from *West and Berry* [1974] and *Lee* [1980]. Data on cyanoacetylene were taken from *Connors et al.* [1974] and *Bruston et al.* [1989], on cyanogen and dicyanogen from *Connors et al.* [1974] and *Nuth and Glicker* [1982]. Acetonitrile data were also taken from *Nuth and Glicker* [1982]. For carbon dioxide the absorption spectrum of *Shemansky* [1972] was used, along with the temperature and pressure dependence of extinction coefficients given by *De More and Patapoff* [1972]. Finally, data reported by *Nicolet* [1981, 1984] were used for water vapor.

In addition to the absorption of solar radiation by gases, we included the absorption due to aerosols at wavelengths shorter than 278 nm in a manner identical to that of *Yung et al.* [1984]. The transmission coefficient is given by

$$T_m(z) = \begin{cases} \exp\left(-\dfrac{240 - z}{H_a} \right) & 40 < z < 240 \text{ km} \\ 1 & z > 240 \text{ km} \end{cases} \tag{5}$$

where $H_a = 50$ km is the aerosol scale height.

Toublanc et al. used a more elaborate treatment, in which they included Rayleigh and Mie scattering. The effect of scattering is to enhance the photodissociation rate compared to the purely absorbing case. At the higher altitudes, as a consequence of backscattering, the photodissociation rates may be larger than the direct solar value, but the effect is of the order of 10% only, which is negligible in view of the larger uncertainties due to the incoming solar flux (and the approximate

Table 1. Photodissociation Processes

	Process	Efficiency
J1a	$CH_4 + h\nu \rightarrow CH_3 + H$	0.49 (1150–1360 Å), 1 ($\lambda >$ 1360 Å)
J1b	$CH_4 + h\nu \rightarrow CH_3^* + H \rightarrow CH + H + H_2$	0.23 (1150–1360 Å), 0 (other)
J1c	$CH_4 + h\nu \rightarrow CH + H + H_2$	0.28 (1150–1360 Å), 0 (other)
J2	$CH_3 + h\nu \rightarrow {}^1CH_2 + H$	1 (at 2160 Å)
J3a	$C_2H_2 + h\nu \rightarrow C_2H + H$	0.30 (1150–1500 Å) 0.08 (1502–2000 Å)
J3b	$C_2H_2 + h\nu \rightarrow C_2 + H_2$	0.10 (1150–2000 Å)
J4a	$C_2H_4 + h\nu \rightarrow C_2H_2 + H_2$	0.51
J4b	$C_2H_4 + h\nu \rightarrow C_2H_2 + 2H$	0.49
J5a	$C_2H_6 + h\nu \rightarrow C_2H_2 + 2H_2$	0.25 (Ly α) 0.27 ($\lambda \neq$ Ly α)
J5b	$C_2H_6 + h\nu \rightarrow C_2H_4 + 2H$	0.30 (Ly α) 0.14 ($\lambda \neq$ Ly α)
J5c	$C_2H_6 + h\nu \rightarrow CH_4 + {}^1CH_2$	0.25 (Ly α) 0.02 ($\lambda \neq$ Ly α)
J5d	$C_2H_6 + h\nu \rightarrow C_2H_4 + H_2$	0.13 (Ly α) 0.56 ($\lambda \neq$ Ly α)
J5e	$C_2H_6 + h\nu \rightarrow CH_3 + CH_3$	0.08 (Ly α) 0.01 ($\lambda \neq$ Ly α)
J6a	$C_4H_2 + h\nu \rightarrow C_4H + H$	0.20 (1150–1650 Å)
J6b	$C_4H_2 + h\nu \rightarrow C_2H_2 + C_2$	0.10 (1150–1650 Å) 0.06 (1652–2050 Å)
J6c	$C_4H_2 + h\nu \rightarrow C_2H + C_2H$	0.03 (1150–1650 Å) 0.01 (1652–2020 Å)
J6d	$C_4H_2 + h\nu \rightarrow C_4H_2^*$	0.67 (1150–1650 Å) 0.93 (1652 2020 Å) 1.00 (2022–2450 Å)
J7a	$CH_3C_2H + h\nu \rightarrow C_3H_3 + H$	0.40
J7b	$CH_3C_2H + h\nu \rightarrow C_3H_2 + H_2$	0.15
J7c	$CH_3C_2H + h\nu \rightarrow CH_3 + C_2H$	0.02
J8a	$C_3H_8 + h\nu \rightarrow C_3H_6 + H_2$	0.33 (Ly α) 0.94 ($\lambda \neq$ Ly α)
J8b	$C_3H_8 + h\nu \rightarrow C_2H_6 + {}^1CH_2$	0.09 (Ly α)
J8c	$C_3H_8 + h\nu \rightarrow C_2H_5 + CH_3$	0.39 (Ly α)
J8d	$C_3H_8 + h\nu \rightarrow C_2H_4 + CH_4$	0.20 (Ly α) 0.06 ($\lambda \neq$ Ly α)
J9	$C_3H_3 + h\nu \rightarrow C_3H_2 + H$	1.00 (1150–1900 Å)
J10a	$CO_2 + h\nu \rightarrow CO + O(^1D)$	$\lambda <$ 1670 Å
J10b	$CO_2 + h\nu \rightarrow CO + O(^3P)$	$\lambda \geq$ 1670 Å
J11a	$H_2O + h\nu \rightarrow H + OH$	0.75 (Ly α) $\lambda \leq$ 1980 Å
J11b	$H_2O + h\nu \rightarrow H_2 + O$	0.25 (Ly α)
J12	$N_2 + h\nu \rightarrow 2N(^2D)$	1.00 (80–800 Å)
J13	$HCN + h\nu \rightarrow H + CN$	1.00 (1150–2200 Å)
J14a	$HC_3N + h\nu \rightarrow C_2H + CN$	0.30 (1150–1500 Å) 0.08 (1502–2000 Å)
J14b	$HC_3N + h\nu \rightarrow H + C_3N$	0.10 (1150–2580 Å)
J15	$C_2N_2 + h\nu \rightarrow CN + CN$	0.3
J16	$C_4N_2 + h\nu \rightarrow C_3N + CN$	0.3
J17a	$CH_3CN + h\nu \rightarrow CH_3 + CN$	0.2
J17b	$CH_3CN + h\nu \rightarrow CH_2CN + H$	0.8

treatment of the diurnal averaging), the values of the cross sections, and the choice of the wavelength step in the integration. At lower altitudes the effect of scattering is primarily to retard the attenuation of the intensity with depth. This effect may be more important and explain differences in photolysis rates (see section 5.1).

3.2. Chemistry

The chemical reactions and their rates used in this study are listed in Table 2. Reaction rates for hydrocarbons have been taken from *Laufer et al.* [1983], *Yung et al.* [1984], *Slagle et al.* [1988], *Romani et al.* [1990], and *Bézard et al.* [1991]; for oxygen compounds, from *Yung et al.* [1984] and *De More et al.* [1985, 1987]; and for nitrogen compounds, from *Yung* [1987], *Marston et al.* [1989a, b], *Marston and Stief* [1989], *Nesbitt et al.* [1990, 1991, 1992], *Tsai and McFadden* [1990], *Sun et al.* [1990], *Balla et al.* [1991], *Barth* [1992], *Yang et al.* [1992], *Monks et al.* [1993], and *Lellouch et al.* [1994].

One important difference between our model and the previous study of *Yung et al.* [1984] arises from the new CH_4 photodissociation paths at Ly α proposed by *Mordaunt et al.* [1993] (see Table 1). Our understanding of the Mordaunt et al. experiment is the following. Mordaunt et al. suggest two different schemes. Their preferred one involves formation of CH_3 and CH, but not of $^1CH_2$ and $^3CH_2$, unlike in the previously accepted schemes:

(J1a) $$CH_4 \rightarrow CH_3 + H$$

(J1b) $$CH_4 \rightarrow CH_3^* + H \rightarrow CH + H + H_2$$

Table 2. Chemical Reactions

	Reaction	Reaction Rate
(R1a)	$^1CH_2 + H_2 \rightarrow CH_3 + H$	$k_{1a} = 7.0 \times 10^{-12}$
(R1b)	$^1CH_2 + H_2 \rightarrow {}^3CH_2 + H_2$	$k_{1b} = 1.0 \times 10^{-12}$
(R2)	$^1CH_2 + CH_4 \rightarrow CH_3 + CH_3$	$k_2 = 2.0 \times 10^{-12}$
(R3)	$CH + CH_4 \rightarrow C_2H_4 + H$	$k_3 = 1.0 \times 10^{-10}$
(R4)	$CH + H_2 + M \rightarrow CH_3 + M$	$k_0 = 3.1 \times 10^{-30} \exp(457/T)$ $k_\infty = 1.5 \times 10^{-11}$
(R5)	$H + CH_3 + M \rightarrow CH_4 + M$	$k_0 = 3.1 \times 10^{-29} \exp(457/T)$ $k_\infty = 1.5 \times 10^{-10}$
(R6)	$CH_3 + CH_3 + M \rightarrow C_2H_6 + M$	See *Slagle et al.* [1988]
(R7)	$H + H + M \rightarrow H_2 + M$	$k_7 = 2.5 \times 10^{-31} T^{-0.6}$
(R8)	$H + C_2H_2 + M \rightarrow C_2H_3 + M$	$k_0 = 6.4 \times 10^{-25} T^{-2} \exp(-1200/T)$ $k_\infty = 9.0 \times 10^{-12} \exp(-1200/T)$
(R9)	$H + C_2H_3 \rightarrow C_2H_2 + H_2$	$k_9 = 1.5 \times 10^{-11}$
(R10)	$H_2 + C_2H_3 \rightarrow C_2H_4 + H$	$k_{10} = 3.0 \times 10^{-13} \exp(-5570/T)$
(R11)	$H + C_2H_4 + M \rightarrow C_2H_5 + M$	$k_0 = 1.1 \times 10^{-23} T^{-2} \exp(-1040/T)$ $k_\infty = 3.7 \times 10^{-11} \exp(-1040/T)$
(R12)	$H + C_2H_5 \rightarrow CH_3 + CH_3$	$k_{12} = 1.9 \times 10^{-10} \exp(-440/T)$
(R13)	$^3CH_2 + H + M \rightarrow CH_3 + M$	$k_0 = 3.1 \times 10^{-30} \exp(457/T)$ $k_\infty = 1.5 \times 10^{-11}$
(R14)	$^3CH_2 + CH_3 \rightarrow C_2H_4 + H$	$k_{14} = 7.0 \times 10^{-11}$
(R15)	$^3CH_2 + C_2H_2 + M \rightarrow CH_3C_2H + M$	$k_0 = 4.0 \times 10^{-26} \exp(634/T)$ $k_\infty = 2.2 \times 10^{-12}$
(R16)	$C_2H + H + M \rightarrow C_2H_2 + M$	$k_0 = 3.1 \times 10^{-30} \exp(457/T)$ $k_\infty = 1.5 \times 10^{-10}$
(R17)	$C_2H + H_2 \rightarrow C_2H_2 + H$	$k_{17} = 5.7 \times 10^{-11} \exp(-1762/T)$
(R18)	$C_2H + CH_4 \rightarrow C_2H_2 + CH_3$	$k_{18} = 2.8 \times 10^{-12} \exp(-250/T)$
(R19)	$C_2H + C_2H_6 \rightarrow C_2H_2 + C_2H_5$	$k_{19} = 1.8 \times 10^{-11} \exp(-302/T)$
(R20)	$C_2H + C_2H_2 \rightarrow C_4H_2 + H$	$k_{20} = 5.0 \times 10^{-11}$
(R21)	$CH_3C_2H + H \rightarrow CH_3 + C_2H_2$	$k_{21} = 9.7 \times 10^{-12} \exp(-1550/T)$
(R22a)	$CH_3C_2H + H + M \rightarrow CH_3 + C_2H_2$	$k_0 = 8.0 \times 10^{-24} T^{-2} \exp(-1225/T)$ $k_\infty = 9.7 \times 10^{-12} \exp(-1550/T)$
(R22b)	$CH_3C_2H + H + M \rightarrow C_3H_5 + M$	$k_0 = 8.0 \times 10^{-24} T^{-2} \exp(-1225/T)$ $k_\infty = 9.7 \times 10^{-12} \exp(-1550/T)$
(R23a)	$C_2H_3 + C_2H_3 \rightarrow C_2H_4 + C_2H_2$	$k_{23a} = 5.3 \times 10^{-12}$
(R23b)	$C_2H_3 + C_2H_3 + M \rightarrow C_4H_6 + M$	$k_0 = 1.3 \times 10^{-22}$ $k_\infty = 9.1 \times 10^{-12}$
(R24)	$C_4H + H_2 \rightarrow C_4H_2 + H$	$k_{24} = 1.9 \times 10^{-11} \exp(-1762/T)$
(R25)	$C_4H + CH_4 \rightarrow C_4H_2 + CH_3$	$k_{25} = 9.3 \times 10^{-13} \exp(-250/T)$
(R26)	$C_4H + C_2H_6 \rightarrow C_4H_2 + C_2H_5$	$k_{26} = 6.0 \times 10^{-12} \exp(-302/T)$
(R27)	$C_4H + H + M \rightarrow C_4H_2 + M$	$k_0 = 1.0 \times 10^{-30} \exp(457/T)$ $k_\infty = 5.0 \times 10^{-11}$
(R28)	$C_4H + C_2H_2 \rightarrow C_6H_2 + H$	$k_{28} = 1.0 \times 10^{-11}$
(R29)	$C_4H + C_4H_2 \rightarrow C_8H_2 + H$	$k_{29} = 1.0 \times 10^{-11}$
(R30)	$C_2H + C_4H_2 \rightarrow C_6H_2 + H$	$k_{30} = 3.1 \times 10^{-11}$
(R31)	$C_4H_2^* + C_4H_2 \rightarrow C_8H_2 + H_2$	$k_{31} = 9.0 \times 10^{-11}$
(R32)	$C_4H_2 + H \rightarrow C_4H_3$	$k_{32} = 1.4 \times 10^{-10} \exp(-1184/T)$
(R33)	$C_4H_3 + H \rightarrow C_4H_2 + H_2$	$k_{33} = 1.2 \times 10^{-11}$
(R34)	$C_4H_3 + H \rightarrow C_2H_2 + C_2H_2$	$k_{34} = 3.3 \times 10^{-12}$
(R35)	$C_2 + H_2 \rightarrow C_2H + H$	$k_{35} = 1.8 \times 10^{-10} \exp(-1469/T)$
(R36)	$C_2 + CH_4 \rightarrow C_2H + CH_3$	$k_{36} = 1.9 \times 10^{-11}$
(R37)	$C_2H + C_2H_4 \rightarrow C_2H_2 + C_2H_3$	$k_{37} = 1.8 \times 10^{-11} \exp(-302/T)$
(R38)	$C_4H + C_2H_4 \rightarrow C_4H_2 + C_2H_3$	$k_{38} = 6.0 \times 10^{-12} \exp(-302/T)$
(R39)	$^1CH_2 + N_2 \rightarrow {}^3CH_2 + N_2$	$k_{39} = 7.9 \times 10^{-12}$
(R40)	$^3CH_2 + {}^3CH_2 \rightarrow C_2H_2 + H_2$	$k_{40} = 5.3 \times 10^{-11}$
(R41a)	$C_2H_5 + CH_3 \rightarrow C_2H_4 + CH_4$	$k_{41a} = 1.7 \times 10^{-12} \exp(-200/T)$
(R41b)	$C_2H_5 + CH_3 + M \rightarrow C_3H_8 + M$	$k_0 = 3.06 \times 10^{-21}$ $k_\infty = 4.2 \times 10^{-11} \exp(-200/T)$
(R42a)	$C_2H_5 + C_2H_3 \rightarrow C_2H_6 + C_2H_2$	$k_{42a} = 6.0 \times 10^{-12}$
(R42b)	$C_2H_5 + C_2H_3 \rightarrow C_2H_4 + C_2H_4$	$k_{42b} = 3.0 \times 10^{-12}$
(R43a)	$C_2H_5 + C_2H_5 \rightarrow C_2H_6 + C_2H_4$	$k_{43a} = 1.7 \times 10^{-12} \exp(-90/T)$
(R43b)	$C_2H_5 + C_2H_5 + M \rightarrow C_4H_{10} + M$	$k_0 = 2.9 \times 10^{-21}$ $k_\infty = 1.3 \times 10^{-11} \exp(-95/T)$
(R44)	$C_3H_3 + H + M \rightarrow CH_3C_2H + M$	$k_0 = 1.7 \times 10^{-26}$ $k_\infty = 1.5 \times 10^{-10}$
(R45a)	$C_3H_5 + H \rightarrow CH_3C_2H + H_2$	$k_{45a} = 1.5 \times 10^{-11}$
(R45b)	$C_3H_5 + H \rightarrow CH_2CCH_2 + H_2$	$k_{45b} = 1.5 \times 10^{-11}$
(R46a)	$C_3H_5 + CH_3 \rightarrow CH_3C_2H + CH_4$	$k_{46a} = 4.5 \times 10^{-12}$
(R46b)	$C_3H_5 + CH_3 \rightarrow CH_2CCH_2 + CH_4$	$k_{46b} = 4.5 \times 10^{-12}$
(R47)	$C_3H_2 + H + M \rightarrow C_3H_3 + M$	$k_0 = 1.7 \times 10^{-26}$ $k_\infty = 1.5 \times 10^{-10}$
(R48)	$^3CH_2 + C_2H_2 \rightarrow$ products	$k_{48} = 5.8 \times 10^{-12}$
(R49)	$C_3H_8 + C_2H \rightarrow C_2H_2 + C_3H_7$	$k_{49} = 1.4 \times 10^{-11}$
(R50)	$C_2H_3 + CH_3 + M \rightarrow C_3H_6 + M$	$k_0 = 1.3 \times 10^{-22}$ $k_\infty = 9.1 \times 10^{-12}$

Table 2. (continued)

	Reaction	Reaction Rate
(R51)	$C_3H_5 + H + M \rightarrow C_3H_6 + M$	$k_0 = 1.0 \times 10^{-28}$ $k_\infty = 1.0 \times 10^{-11}$
(R52)	$C_2H_3 + CH_3 \rightarrow C_2H_2 + CH_4$	$k_{52} = 9.1 \times 10^{-12}$
(R53)	$C_2H_3 + C_2H_5 + M \rightarrow C_4H_8 + M$	$k_{53} = k_{50}$
(R54)	$C_3H_5 + CH_3 + M \rightarrow C_4H_8 + M$	$k_{54} = k_{50}$
(R55)	$C_4H_2 + H + M \rightarrow C_4H_3 + M$	$k_0 = 1.0 \times 10^{-28}$ $k_\infty = 2.0 \times 10^{-12}$
(R56)	$C_4H_2^* \rightarrow C_4H_2 + h\nu$	$k_{56} = 1.0 \times 10^3$
(R57)	$CH + C_2H_4 \rightarrow CH_3C_2H + H$	$k_{57} = 5.5 \times 10^{-11} \exp(173/T)$
(R58)	$O(^1D) + N_2 \rightarrow O(^3P) + N_2$	$k_{58} = 1.8 \times 10^{-11} \exp(107/T)$
(R59)	$O(^1D) + CH_4 \rightarrow OH + CH_3$	$k_{59} = 1.4 \times 10^{-10}$
(R60)	$O(^3P) + {}^3CH_2 \rightarrow CO + 2H$	$k_{60} = 8.3 \times 10^{-11}$
(R61)	$OH + CH_4 \rightarrow H_2O + CH_3$	$k_{61} = 2.4 \times 10^{-12} \exp(-1710/T)$
(R62)	$OH + {}^3CH_2 \rightarrow CO + H_2 + H$	$k_{62} = 5.0 \times 10^{-12}$
(R63)	$OH + CH_3 \rightarrow CO + H_2 + H_2$	$k_{63} = 6.7 \times 10^{-12}$
(R64)	$OH + CO \rightarrow CO_2 + H$	$k_{64} = 6.0 \times 10^{-13}[(0.25 + 1.82 \times 10^{-20}\text{M})/(1 + 1.82 \times 10^{-20}\text{M})]$
(R65)	$CO + H + M \rightarrow HCO + M$	$k_{65} = 2.0 \times 10^{-33} \exp(-850/T)$
(R66)	$H + HCO \rightarrow H_2 + CO$	$k_{66} = 3.0 \times 10^{-10}$
(R67)	$HCO + HCO \rightarrow H_2CO + CO$	$k_{67} = 6.3 \times 10^{-11}$
(R68)	$O(^1D) + H_2 \rightarrow H + OH$	$k_{68} = 1.0 \times 10^{-10}$
(R69)	$O(^1D) \rightarrow O(^3P) + h\nu$	$k_{69} = 6.7 \times 10^{-3}$
(R70)	$OH + OH \rightarrow H_2O + O(^3P)$	$k_{70} = 4.2 \times 10^{-12} \exp(-242/T)$
(R71)	$OH + H_2 \rightarrow H_2O + H$	$k_{71} = 6.1 \times 10^{-12} \exp(-2030/T)$
(R72)	$O(^3P) + C_2H_2 \rightarrow CO + {}^3CH_2$	$k_{72} = 2.9 \times 10^{-11} \exp(-1600/T)$
(R73)	$O(^3P) + C_2H_4 \rightarrow CH_3 + HCO$	$k_{73} = 5.3 \times 10^{-12} \exp(-640/T)$
(R74)	$CO + O(^3P) + M \rightarrow CO_2 + M$	$k_{74} = 6.5 \times 10^{-33} \exp(-2180/T)$
(R75)	$N(^2D) + N_2 \rightarrow N(^4S) + N_2$	$k_{75} = 1.6 \times 10^{-14}$
(R76)	$N(^2D) + H_2 \rightarrow NH + H$	$k_{76} = 5.0 \times 10^{-12}$
(R77)	$N(^2D) + CH_4 \rightarrow NH + CH_3$	$k_{77} = 3.0 \times 10^{-12}$
(R78)	$N(^2D) + C_2H_2 \rightarrow CHCN + H$	$k_{78} = 1.0 \times 10^{-11}$
(R79)	$N(^2D) + C_2H_4 \rightarrow NH + C_2H_3$	$k_{79} = 1.2 \times 10^{-12}$
(R80)	$N(^2D) + C_2H_6 \rightarrow NH + C_2H_5$	$k_{80} = 3.0 \times 10^{-12}$
(R81)	$N(^4S) + CH_3 \rightarrow H_2CN + H$	$k_{81} = 6.4 \times 10^{-11}$
(R82)	$N(^4S) + {}^3CH_2 \rightarrow HCN + H$	$k_{82} = 1.6 \times 10^{-11}$
(R83)	$N(^4S) + C_2H_3 \rightarrow HCN + {}^3CH_2$	$k_{83} = 4.4 \times 10^{-11}$
(R84)	$N(^4S) + C_2H_3 \rightarrow NH + C_2H_2$	$k_{84} = 6.6 \times 10^{-11}$
(R86)	$N(^4S) + C_2H_5 \rightarrow H_2CN + CH_3$	$k_{86} = 4.4 \times 10^{-11}$
(R87)	$N(^4S) + C_2H_5 \rightarrow NH + C_2H_4$	$k_{87} = 6.6 \times 10^{-11}$
(R88)	$N(^4S) + NH \rightarrow N_2 + H$	$k_{88} = 1.1 \times 10^{-11} T^{0.5}$
(R89)	$N(^2D) \rightarrow N(^4S) + h\nu$	$k_{89} = 1.07 \times 10^{-5}$
(R90)	$NH + H \rightarrow N(^4S) + H_2$	$k_{90} = 1.7 \times 10^{-12} T^{0.68} \exp(-950/T)$
(R91)	$NH + C_2H_3 \rightarrow$ products	$k_{91} = 4.0 \times 10^{-11}$
(R92)	$NH + C_2H_5 \rightarrow$ products	$k_{92} = 4.0 \times 10^{-11}$
(R93)	$NH + CH_3 \rightarrow CH_2NH + H$	$k_{93} = 4.0 \times 10^{-11}$
(R94)	$NH + CH_3 \rightarrow N(^4S) + CH_4$	$k_{94} = 4.0 \times 10^{-11}$
(R95)	$NH + NH + M \rightarrow N_2 + H_2$	$k_0 = 1.0 \times 10^{-33}$ $k_\infty = 1.0 \times 10^{-14}$
(R96)	$HCN + C_2H_3 \rightarrow C_2H_3CN + H$	$k_{96} = 1.1 \times 10^{-12} \exp(-900/T)$
(R97)	$HCN + C_2H \rightarrow HC_3N + H$	$k_{97} = 1.1 \times 10^{-11}$
(R98)	$H_2CN + N(^4S) \rightarrow HCN + NH$	$k_{98} = 3.9 \times 10^{-11}$
(R99)	$H_2CN + H \rightarrow HCN + H_2$	$k_{99} = 7.0 \times 10^{-11}$
(R100)	$CN + CH_4 \rightarrow HCN + CH_3$	$k_{100} = (1 - \alpha) \times 10^{-19} T^{2.64} \exp(220/T)$[a]
(R101)	$CN + CH_4 \rightarrow H + CH_3CN$	$k_{101} = \alpha \times 10^{-19} T^{2.64} \exp(220/T)$[a]
(R102)	$CN + C_2H_2 \rightarrow HC_3N + H$	$k_{102} = 5.67 \times 10^{-9} T^{0.55} \exp(-4/T)$
(R103)	$CN + C_2H_4 \rightarrow HCN + C_2H_3$	$k_{103} = 1.08 \times 10^{-10} \exp(172/T)$
(R104)	$CN + C_2H_4 \rightarrow C_2H_3CN + H$	$k_{104} = 2.7 \times 10^{-11} \exp(172/T)$
(R105)	$CN + C_2H_6 \rightarrow HCN + C_2H_5$	$k_{105} = (1 - \alpha) \times 2.0 \times 10^{-19} T^{2.77} \exp(900/T)$[a]
(R106)	$CN + C_2H_6 \rightarrow CH_3CN + CH_3$	$k_{106} = \alpha \times 2.0 \times 10^{-19} T^{2.77} \exp(900/T)$[a]
(R107)	$CN + HCN \rightarrow C_2N_2 + H$	$k_{107} = 6.31 \times 10^{-17} T^{1.57} \exp(-50/T)$
(R108)	$C_3N + CH_4 \rightarrow HC_3N + CH_3$	$k_{108} = 5.0 \times 10^{-14}$
(R109)	$C_3N + C_2H_6 \rightarrow HC_3N + C_2H_5$	$k_{109} = 1.0 \times 10^{-11}$
(R110)	$HC_3N + H + M \rightarrow H_2C_3N + M$	$k_0 = 6.4 \times 10^{-25} T^{-2} \exp(-1200/T)$ $k_\infty = 9.2 \times 10^{-12} \exp(-1200/T)$
(R111)	$HC_3N + CN \rightarrow H + C_4N_2$	$k_{111} = 1.0 \times 10^{-11}$
(R112)	$CHCN + N(^4S) \rightarrow C_2N_2 + H$	$k_{112} = 1.0 \times 10^{-12}$
(R113)	$C_2N_2 + H + M \rightarrow HC_2N_2 + M$	$k_0 = 6.4 \times 10^{-25} T^{-2} \exp(-1200/T)$ $k_\infty = 1.5 \times 10^{-15}$
(R114)	$CHCN + CHCN \rightarrow C_4N_2 + H_2$	$k_{114} = 5.0 \times 10^{-11}$

All values quoted are in the cm s system. Three-body reaction rates are calculated according to the expression $k = k_0 k_\infty / (k_0 M + k_\infty)$.

[a]See text ($\alpha = 0.05$ for $CN + CH_4$ and 0.035 for $C_2H_6 + CN$).

(J1c) $CH_4 \rightarrow CH + H + H_2$

At Ly α, the quantum yields are measured to be 0.49, 0.28, and 0.23, respectively. We adopt these yields at wavelengths $\leq$136 nm. Above 136 nm, the second and third paths are not energetically possible, and CH_4 entirely dissociates to CH_3 and H (D. Strobel, private communication, 1995). (*Toublanc et al.* [1995] also quoted Mordaunt et al.'s work, but in most of their study, they used the other scheme, with abundant production of $^1CH_2$ and $^3CH_2$ (quantum yields 0.24 and 0.25, respectively). They nonetheless also ran their model with the above reactions for comparison and found no significant differences in the results.)

Based on these paths and on an investigation of the main reactions controlling the production and loss of the atmospheric compounds, it is possible to synthetically view the chemistry in terms of a limited number of chemical cycles.

The first cycle, initiated by the production of CH, leads to the production of ethylene in the mesosphere and thermosphere.

Cycle 1

(J1b + J1c) $CH_4 + h\nu \rightarrow CH + H + H_2$

(R3) $CH_4 + CH \rightarrow C_2H_4 + H$

Net $2CH_4 \rightarrow C_2H_4 + 2H + H_2$

The direct production of CH_3 from the photolysis of CH_4 permits the formation of ethane in the mesosphere and lower thermosphere ($\leq$800 km) (in addition to its formation in the stratosphere through catalytic processes).

Cycle 2

(J1a) $2[CH_4 + h\nu \rightarrow CH_3 + H]$

(R6) $CH_3 + CH_3 + M \rightarrow C_2H_6 + M$

Net $2CH_4 \rightarrow C_2H_6 + 2H$

Once ethylene is formed, its photolysis leads to acetylene through (J4a) and (J4b):

$$C_2H_4 \rightarrow C_2H_2 + H_2 \text{ (or } + 2H)$$

Combining this reaction with cycle 1, we obtain

Cycle 3a $2CH_4 \rightarrow C_2H_2 + 2H + 2H_2$

or

Cycle 3b $2CH_4 \rightarrow C_2H_2 + 4H + H_2$

Methyl acetylene formation occurs in the mesosphere according to (J5c) + (R39) + (R15) + cycle 2 + cycle 3b, that is,

Cycle 4 $3CH_4 \rightarrow CH_3C_2H + 6H + H_2$

where the production of $^1CH_2$ from ethane photolysis is a crucial step.

Propane production takes place in the stratosphere and is controlled by (J3a) + (R19) + (J1a):

$$CH_4 + C_2H_6 \rightarrow C_3H_8 + 2H$$

or, equivalently, (J3a) + (R19) + (J1a) + cycle 2:

Cycle 5 $3CH_4 \rightarrow C_3H_8 + 4H$

Once acetylene is formed in the mesosphere, it diffuses downward and is lost by (J3a) + (R20):

$$2C_2H_2 \rightarrow C_4H_2 + 2H$$

In terms of methane loss, the diacetylene formation can therefore be expressed by (J2a) + (R20) + cycle 3b

Cycle 6 $4CH_4 \rightarrow C_4H_2 + 10H + 2H_2$

It can be seen that the production of the different hydrocarbons involves a significant consumption of CH_4 and an extremely high production of H and H_2. Most of the H is released in the stratosphere as a consequence of the photosensitized dissociation of CH_4 by (R3). Note, however, that its destruction, governed by the conversion of H to H_2 catalyzed by C_2H_2, C_4H_2, and HCN, is located in the same atmospheric region.

Alkanes undergo photosensitized dissociation from H abstraction by several radicals. For CH_4, C_2H_6, and C_3H_8, this process occurs in the stratosphere, where the catalysts are C_2H and C_4H. In the case of methane, this mechanism is also possible in the thermosphere and mesosphere with $N(^4S)$, $N(^2D)$, $O(^1D)$ and OH as catalysts.

The insertion reactions leading to the formation of polyynes can be schematized by the cycles formed from (J6a) + (R28) and (J3a) + (R30):

Cycle 7 $C_4H_2 + C_2H_2 \rightarrow C_6H_2 + 2H$

catalyzed either by C_2H or by C_4H, and by (J6a) + (R29), giving rise to

Cycle 8 $2C_4H_2 \rightarrow C_8H_2 + 2H$

and representing a chemical sink of acetylene and diacetylene in the mesosphere.

Sources of oxygen in Titan's atmosphere may be external (influx of oxygen-bearing material), and/or internal (supply of CO from an oceanic reservoir [*Dubouloz et al.*, 1989]). The external source is necessary to produce the OH atoms required for the CO_2 formation (see section 3.3). The formation of carbon dioxide from water vapor and carbon monoxide may be written as (J11a) + (R64):

Cycle 9 $H_2O + CO \rightarrow CO_2 + 2H$

while the recycling of carbon monoxide occurs by (J10a) + (J10b) + (R58) + (R60) + (R72):

Cycle 10 $2CO_2 + C_2H_2 \rightarrow 4CO + 2H$

The dissociation of N_2 by any of the processes described in section 3.4 results in the formation of nitrogen atoms. $N(^2D)$ and $N(^4S)$, in addition to catalyzing the CH_4 dissociation in the thermosphere, play a crucial role in the production of HCN according to

Cycle 11 $2CH_4 + N_2 \rightarrow 2HCN + 2H_2 + 2H$

either by means of H_2CN ((R98) or (R99)) or directly by CH_3/CH_2 ((R81)/(R82)).

The recent detection of acetonitrile [*Bézard et al.*, 1993] requires finding a mechanism for producing this species. We propose two different schemes:

Cycle 12

(J13) $HCN + h\nu \rightarrow H + CN$

(R101) $CN + CH_4 \rightarrow CH_3CN + H$

Net $HCN + CH_4 \rightarrow CH_3CN + H$

Cycle 13

(J13) $HCN + h\nu \rightarrow H + CN$

(J1a) $2[CH_4 \rightarrow CH_3 + H]$

(R6) $2CH_3 + M \rightarrow C_2H_6 + M$

(R106) $CN + C_2H_6 \rightarrow CH_3CN + CH_3$

Net $HCN + 2CH_4 \rightarrow CH_3CN + CH_3 + 3H$

and we will study them separately.

Hydrogen cyanide also participates in the formation of HC_3N in two different ways, catalyzed by either C_2H (in the stratosphere) or CN (in the thermosphere and mesosphere). The reactions are (J3a) + (R97) and (J13) + (R102), giving as a net result

Cycle 14 $HCN + C_2H_2 \rightarrow HC_3N + 2H$

The production of cyanogen is mainly controlled by the sequence (J12) + (R75) + (R78) + (R112), that is, $N_2 + C_2H_2 \rightarrow C_2N_2 + 2H$ (cycle 15), and $N_2 + 2C_2H_2 \rightarrow C_4N_2 + 2H + H_2$ (cycle 16 = (J12) + (R78) + (R114)) is the preferred mechanism for dicyanogen.

3.3. Oxygen Source

The presence of CO_2 in Titan's stratosphere implies a source of OH, as CO_2 is formed through

$$CO + OH \rightarrow CO_2 + H$$

where CO is either provided from the surface or produced in reactions between OH and CH_3/CH_2 or between $O(^3P)$ and $^3CH_2$.

This issue was investigated in detail by *Samuelson et al.* [1983] and *Yung et al.* [1984], who showed that the most efficient source of OH was the photolysis of H_2O produced from ablation of micrometeorites in the upper atmosphere. (An alternate source of OH is the electron impact dissociation of CO, producing $O(^1D)$, which reacts with CH_4 to produce OH.) This scheme for the production of CO_2 requires that CO must be abundant enough to compete with CH_4, C_2H_2, and some radicals in reactions with OH. Because the lifetime of CO_2 against photolysis is very short (of the order of 5×10^4 years according to *Samuelson et al.* [1983]), the source of oxygen in the form of OH must be continuous. *Samuelson et al.* [1983] found that a supply of 6.1×10^5 O atoms cm^{-2} s^{-1}, referred to the surface, was necessary to match their measured CO_2 mixing ratio of 1.5×10^{-9}. This flux was obtained for a CO mixing ratio of 1.1×10^{-4}, a value necessary for CO to be in steady state. *Yung et al.* [1984] essentially confirmed this result by requiring an oxygen inward flux of 6.1×10^5 cm^{-2} s^{-1} and a CO mixing ratio of 1.8×10^{-4}. Recently, *Toublanc et al.* [1995] used a downward flux of 1.5×10^6 O atoms cm^{-2} s^{-1} and required a CO mixing ratio of 10^{-4} in order to match the lower stratosphere CO_2 abundance of 1.4×10^{-8} [*Coustenis et al.*, 1989].

All previous models have modeled the O source as a downward flux at the top boundary. *English et al.* [1996] recently developed a model to calculate the interplanetary dust flux into Titan's atmosphere. This model computes the input of meteoritic material at Titan and, by combining the results with an ablation model, it allows us to estimate leading and trailing deposition profiles at Titan for 100% water ice interplanetary meteoroids. The peak of ablation (and hence of water deposition) occurs at an altitude of 700 km, and the leading deposition rate is 20 times larger than the trailing. As an improvement with respect to earlier photochemical models, we have introduced in our code the ablation profile computed by *English et al.* [1996] for the leading side (shown in Figure 1). This profile corresponds to an integrated H_2O deposition rate of 3.1×10^6 cm^{-2} s^{-1} (referred to the tropopause). We also investigated variations in this ablation profile (see section 5).

3.4. N_2 Dissociation

The formation of nitrile compounds in Titan's reducing atmosphere is initiated by the dissociation of N_2. In particular, the main reactions forming HCN, the precursor molecule of several nitriles, are $^3CH_2 + N(^4S) \rightarrow HCN + H$ and $CH_3 + N(^4S) \rightarrow H_2CN + H \rightarrow HCN + H_2$. Ground-state atomic nitrogen is produced directly from the dissociation of N_2, which can proceed through electron impact, N_2^+ dissociative recombination, and galactic cosmic ray absorption (GCR). It can also be produced from relaxation of excited nitrogen $N(^2D)$ or reaction of the latter with N_2. $N(^2D)$ is formed in all of the above dissociation processes. In addition (and principally), $N(^2D)$ is produced in the photolysis of N_2.

Photodissociation of molecular nitrogen is only effective at EUV wavelengths ($\lambda < 80$ nm) where the solar flux is small. Nevertheless, this mechanism is the dominant process above ~700 km. At lower altitudes the main source of atomic nitrogen is provided by GCR dissociation. We used a model of $N(^4S)$ and $N(^2D)$ production from GCR cosmic ray impact similar to models developed by *Moses et al.* [1989, 1992] and *Lellouch et al.* [1994] for Neptune's atmosphere. In this simplified treatment the secondary particle cascade resulting from interactions between GCR and atmospheric nuclei is neglected. Also, the interaction cross sections are assumed to be independent of energy. The method consists of, first, evaluating the ionization rate, according to the expression suggested by *Moses et al.* [1992], and then calculating the $N(^4S)$ and $N(^2D)$ production rate by considering the different paths of ionization and dissociation of N_2 by the electrons produced by the collision of cosmic rays on atmospheric nuclei. The relative yields for the production of N_2^+, $N(^2D)$, and $N(^4S)$ are taken from *Lellouch et al.* [1994].

Capone et al. [1983] developed a much more sophisticated model for the interaction of GCRs with Titan's atmosphere, in which they considered the entire particle cascade (protons, neutrons, pions, muons) and solved a Boltzmann transport equation to obtain the distribution of all these particles. *Lellouch et al.* [1994] adapted their Neptune GCR model to Titan and compared the results with those of *Capone et al.* [1983]. Good agreement was found for the peak altitude (near 105 km) and the N peak production (about 20 cm^{-3} s^{-1}), while the *Lellouch et al.* [1994] model strongly underpredicted the production below the peak (as a result of their neglect of the particle cascade). The most serious and surprising discrepancy was found above the peak, with the production in the Capone et al. model decreasing faster. As a further check, Lellouch et al. adapted their code to the terrestrial atmosphere and concluded that their altitude dependence above the peak was correct, suggesting a potential (but not well understood) problem in the *Capone et al.* [1983] model.

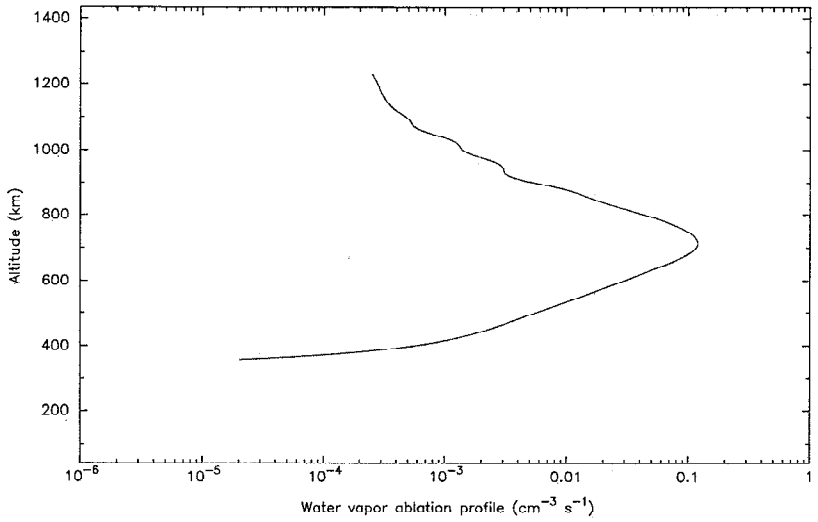

Figure 1. The nominal H_2O deposition rate used in the model, taken from the ablation model of *English et al.* [1996].

Other potential sources of atomic nitrogen include the dissociation of N_2 by magnetospheric electrons and protons and by interplanetary electrons [*Sagan and Thompson*, 1984]. Sagan and Thompson showed that only the effect of magnetospheric electrons can be important compared to solar UV and GCRs, and in a limited altitude range only (500–750 km). Our preliminary modeling of this process supports this finding. *Toublanc et al.* [1995] also mention (D. Strobel, private communication, 1995) that the flux of $N(^4S)$ and $N(^2D)$ due to magnetospheric electrons is about 7×10^7 cm^{-2} s^{-1}, i.e., ~10 times less than the production due to direct EUV photolysis. Because we also used a simplified description of the UV dissociation (not considering the dissociation by photoelectrons, which are potentially more important than magnetospheric electrons), we did not include the effect of magnetospheric electrons in our model. Figure 2 shows the volumic N_2 dissociation rates for the EUV and GCR sources.

3.5. Condensation Processes

Most of the hydrocarbons and nitriles, and CO_2, condense out in Titan's lower stratosphere. The condensation loss process is based on the diffusive growth of ice crystals. We here compute condensation rates following the method outlined by *Romani et al.* [1993]. The diffusive mass growth rate (g s^{-1}) per crystal is taken from *Pruppacher and Klett* [1980]:

$$\frac{dm}{dt} \approx \frac{4\pi a s V_p D' M}{RT} \tag{6}$$

where a is the crystal radius (for a spherical crystal), V_p and M are the vapor pressure and the molecular weight of the condensing species, respectively, and s is the supersaturation (i.e., $s = (p_i - V_p)/V_p$, where p_i is the gas partial pressure). From this, the condensation loss rate (cm^{-3} s^{-1}) can be calculated as

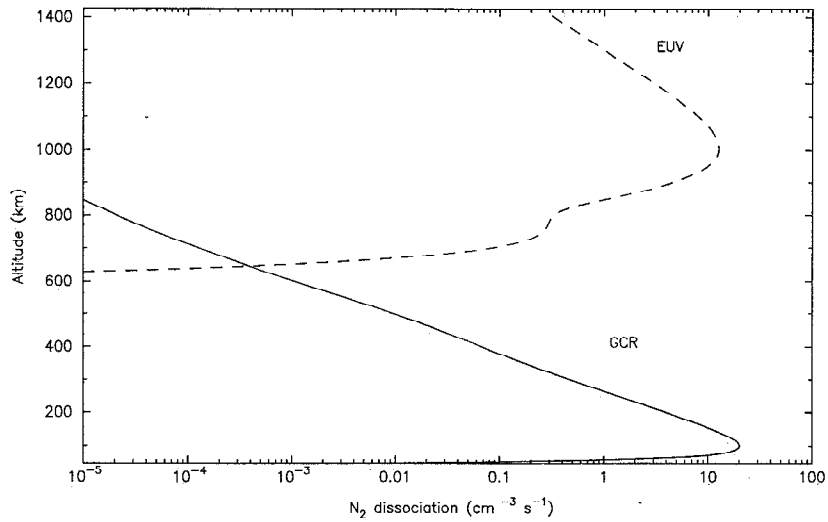

Figure 2. N_2 dissociation rates from EUV absorption and GCR impact.

Table 3. Vapor Pressures

Species	Expression	Temperature Range, K
CH_4	$4.4205070 - (453.92414/T) - (4055.6016/T^2) + (115351.19/T^3) - (1165560.7/T^4)$	67–90.65
C_2H_6	$10.01 - [1085.0/(T - 0.561)]$	30–90
C_2H_6	$5.9366 - (1086.17/T) + 3.83464 \log_{10}(1000/T)$	90–140
C_2H_2	$6.09748 - (1644.1/T) + 7.42346 \log_{10}(1000/T)$	80–145
C_2H_4	$2.25852 - (997.8760/T) + 4.544486 \log_{10}(T) - 0.0179T$	<104
C_2H_4	$50.79 - (1703.0/T) - 17.141 \log_{10}(T)$	104–120
C_2H_4	$6.74756 - [585/(T - 18.16)] - 17.141 \log_{10}(T)$	>120
CH_3C_2H	$5.5206 - (1374.76/T) + 1.2665 \log_{10}(T)$	162–198.7
C_4H_2	$5.3817 - (3300.5/T) + 16.63415 \log_{10}(1000/T)$	127–249
C_3H_8	$8.16173 - (1176.0/T)$	105–165
CO_2	$9.845 - (1390.0/T) + 0.0799 \log_{10}(T)$	139–168.4
HCN	$11.41 - (2318.0/T)$	131.9–168.4
HC_3N	$6.222 - (1913.0/T)$	See *Sagan and Thompson* [1984]
C_2N_2	$7.454 - (1832.0/T)$	177–196
C_4N_2	$8.269 - (2155.0/T)$	147–162
CH_3CN	$8.458 - (1911.7/T)$	226–256.7

$$l_c = \frac{dm}{dt}\frac{N_{Av}}{M}N_{crys} \quad (7)$$

where N_{Av} is the Avogadro's number and N_{crys} is the number of crystals per cm^3. D' is the molecular diffusion coefficient of the condensing species corrected for gas kinetic effects and can be expressed as

$$D' = \frac{D}{[a/(a+\lambda)] + [D/(a\alpha)][(2\pi M)/(RT)]^{1/2}} \quad (8)$$

where D is the standard molecular diffusion coefficient, λ is the mean free path of the atmospheric molecules, and α is the sticking efficiency (we assumed $\alpha = 1$). In Titan's conditions, the second term in the denominator dominates, and the crystal grows proportional to a^2.

Saturation laws used for each molecule are given in Table 3, based on information given by *Sagan and Thompson* [1984], *Reid et al.* [1988], and *Moses et al.* [1992] and from fitting of the three coldest data points given in the *Handbook of Chemistry and Physics* [*Weast et al.*, 1987–1988].

Computing the condensation rates requires a number density profile for the ice crystals. Here, rather than calculating N_{crys} self-consistently from the crystal photochemical production rate and the associated falling rates, as *Romani et al.* [1993] did, we made use of aerosol distributions calculated by earlier modelers. Specifically, we considered (1) an aerosol distribution from *Cabane et al.* [1992], provided by E. Chassefière (private communication, 1993), and (2) an aerosol distribution from *Frère et al.* [1990]. The difference between the two is that while the distribution from Cabane et al. simply considers the growth of aerosols from coagulation (up to radii of about 0.2 μm), that from *Frère et al.* [1990] additionally includes the condensation of the major hydrocarbons and HCN on the aerosol nuclei, resulting in much larger and much less abundant ice particles. However, the condensation rate ((6)–(8)) is proportional to the a $^2N_{crys}$ product, a term which, within a factor of 1.6, is the same for the two distributions we considered. The effect of this difference on the gaseous profiles is entirely negligible because supersaturations are very small (10^{-3}–10^{-6} at most levels). For example, for a nominal supersaturation of 10^{-4}, an error by a factor of 10 in the aerosol profiles (and therefore on the supersaturation factor) results in a 0.1% error in the gaseous mixing ratio. These small supersaturations justify the simplified description adopted by previous photochemical modelers [*Yung et al.*, 1984; *Toublanc et al.*, 1995], in which the condensing compounds are assumed to follow their saturation law below the condensation level. However, the advantage of our treatment is that it allows us to compute condensation fluxes (Φ_c) and to check the mass conservation (i.e., compare the integrated net production with Φ_c) for the individual species (see Table 5 and section 5). The model calculates the number densities as a function of the altitude, and when the obtained mixing ratio is larger than allowed by the saturation law, the loss due to condensation is taken into account. Note that for some species, supersaturations are even smaller than 10^{-4}, and in this case, even convergence of the mixing profiles to 1 part in 10^4 is not sufficient (see section 5).

4. Diffusion Processes

Vertical transport affects the atmospheric composition. In the flux equation (2), the D_i and K coefficients characterize

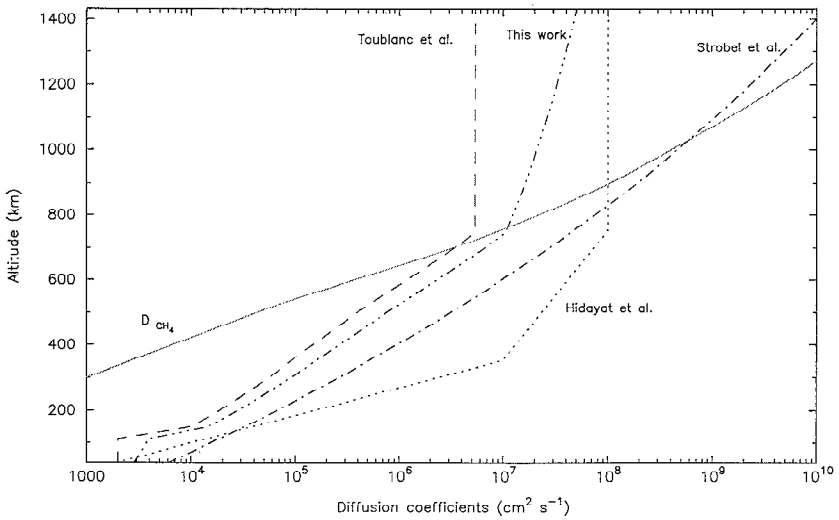

Figure 3. Various eddy diffusion coefficient profiles. The profile labeled Hidayat et al. is the one inferred by T. Hidayat et al. (submitted paper, 1996) below 400 km from HCN observations and extrapolated above this altitude as described in the text. Also shown is the molecular diffusion coefficient for CH_4.

molecular and turbulent (eddy) diffusion, respectively. Molecular diffusion coefficients were taken from *Chamberlain and Hunten* [1987] and *Banks and Kockarts* [1973]. The thermal diffusion factor α_i was assumed to be zero except for atomic and molecular hydrogen, for which we take $\alpha_i = 0.4$. The adopted profile for the CH_4–N_2 molecular diffusion coefficient is shown in Figure 3.

There is no consensus to date on the magnitude and variation with altitude of the eddy diffusion coefficient K in Titan's atmosphere. *Allen et al.* [1980] used an eddy K profile based on earlier work by *Yung and Strobel* [1980] on Jupiter's atmosphere. Further information on K has been inferred either from fitting of the CH_4 and C_2 hydrocarbon abundances in the thermosphere or from fitting of vertical distributions in the stratosphere/mesosphere, primarily HCN. *Smith et al.* [1982] used methane and C_2 hydrocarbon mixing ratios derived from the Voyager/UVS spectra and a simplified, isothermal, photochemical model, to derive a homopause altitude of ~925 km and a value of K equal to 1×10^8 cm^2 s^{-1} at this altitude. *Steiner and Bauer* [1990] used a similar method and found that the homopause could lie anywhere between 500 and 950 km with a preferred altitude of 660 km. Subsequently, *Strobel et al.* [1992] reanalyzed the UVS data in terms of the CH_4 thermospheric mixing profile and inferred an eddy diffusion profile in the form $K(z) = K_0 \exp[\xi(z)/1.6]$, where $\xi(z)$ is the normalized geopotential altitude with respect to the homopause ($z_0 = 985$ km) and K_0, the value of K at z_0, is equal to 4×10^8 cm^2 s^{-1}. *Yung et al.* [1984], in their detailed photochemical model, assumed a complex shape for K, with two stagnant regions, and adjusted the magnitude of K in the different regions so as to obtain a reasonable agreement with the then available analyses of the Voyager observations. *Tanguy et al.* [1990] pointed out that a modification of the eddy diffusion profile adopted by *Yung et al.* [1984] below 320 km was necessary to reproduce the HCN vertical profile determined from their millimeter observations. *Toon et al.* [1992] proposed another modification of the Yung et al. profile in order to fit the HCN profile and to calculate a haze distribution consistent with the ultraviolet and the near-infrared geometric albedo. *Toublanc et al.* [1995] again used the HCN profile of *Tanguy et al.* [1990] as the prime observational constraint, but they worked with different (smaller) downward fluxes of N(^4S) and N(^2D) than Tanguy et al. and were led to yet another K profile. Most recently, T. Hidayat et al. (Millimeter and submillimeter heterodyne observations of Titan: Retrieval of the vertical profile of HCN and the $^{12}C/^{13}C$ ratio, submitted to *Icarus*, 1996; hereinafter cited as submitted paper.) reported new millimeter observations of HCN, providing an improved determination of the HCN profile at 100–400 km, from which they proposed a new K profile at 100–400 km with much larger values than in all earlier profiles at 200–400 km.

In this complicated situation, our approach has been to test some of the proposed K profiles. Specifically, we have run our photochemical model with the eddy diffusion profiles of *Strobel et al.* [1992], *Toublanc et al.* [1995], and T. Hidayat et al. (submitted paper, 1996). In the latter case, we extrapolated the profile of Hidayat et al. above 350 km, and up to 750 km, by assuming $K = A \exp(z/B)$ with $A = 1.532 \times 10^6$ cm^2 s^{-1} and $B = 174.6$ km, while above 750 km we took a constant value $K = 1 \times 10^8$ cm^2 s^{-1} (see Figure 3). These tests led us to propose another profile of K, although we also concluded that with the current chemistry it is not possible to fit all observational constraints with a single K profile. Figure 3 shows the various K profiles along with the CH_4–N_2 molecular diffusion coefficient.

5. Results

5.1. Photodissociation Coefficients

Titan's atmosphere is very opaque for UV radiation. At Ly α and $\lambda < 140$ nm, the opacity is dominated by methane, and light can penetrate down to ~600 km. At longer wavelengths ($140 < \lambda < 180$ nm), radiation is not absorbed by methane but only by some of the heavier hydrocarbons and can therefore reach lower atmospheric levels (~200 km). At even longer wavelengths ($\lambda > 180$ nm), atmospheric gases become progressively transparent, and aerosols are the main absorbers at $\lambda > 210$ nm.

These considerations can be seen in the structure of the photodissociation coefficients (Figure 4). The photodissocia-

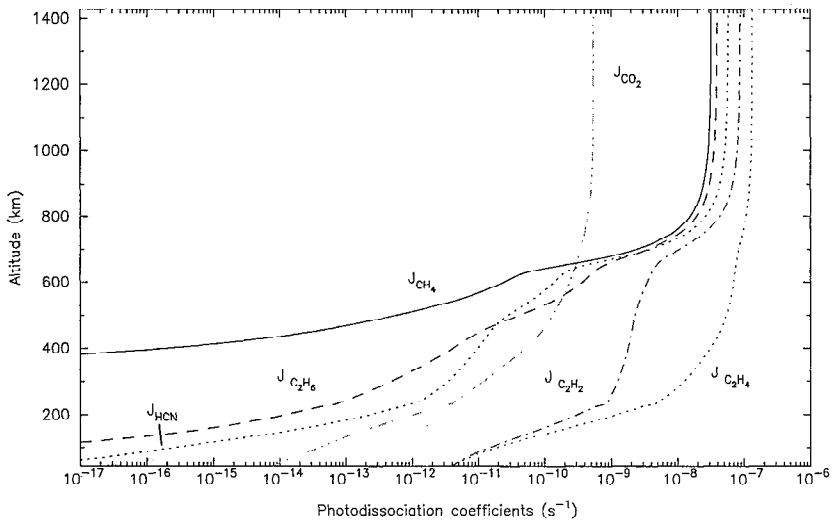

Figure 4. Total photodissociation coefficients of CH_4, C_2H_6, C_2H_2, C_2H_4, CO_2, and HCN.

tion coefficient of methane shows a sharp decrease near 700 km, corresponding to optical depth unity for Ly α. However, significant photolysis occurs down to 500 km through absorption between 120 and 140 nm. Photodissociation coefficients for other gases (e.g., C_2H_6, HCN ...) which mostly absorb in the same spectral regions as CH_4 (i.e., at $\lambda < 140$ nm) show a similar altitude dependence because of the shielding by CH_4. On the other hand, for gases which absorb primarily at $\lambda > 140$ nm (e.g., C_2H_4, CO_2) the decrease of their photodissociation coefficients occurs at deeper levels (near 300 km), corresponding to the extinction of the solar light at 150–210 nm due to their combined opacity. Finally, species like C_2H_2 and C_4H_2 absorb significantly throughout the 100- to 200-nm region, which results in a more complicated structure in their J_i, with the attenuation occurring in two steps, first near 700 km (due to CH_4 absorption), and then near 300 km. Therefore, most species undergo a significant photolysis also at mesospheric levels, releasing short-lived species which are responsible for most of the catalytic cycles acting in this region. A consequence is that the H and H_2 production occurs not only at thermospheric levels, as a result of the direct photolysis of methane, but also in the mesosphere, owing to these catalytic cycles. We find that the relative importance of these two processes (in terms of the total production) is about 30%:70%.

Comparing our photodissociation coefficients with those shown by *Yung et al.* [1984] and *Toublanc et al.* [1995] shows a good overall consistency in the optically thin region of the atmosphere. At deeper regions, our J profiles are similar to those of Yung et al. but decrease faster than those of *Toublanc et al.* [1995]. For example, for HCN, our photolysis rate at 300 km is 3.0×10^{-12} s^{-1} versus 1.0×10^{-11} s^{-1} for Yung et al. and 5.0×10^{-10} s^{-1} for Toublanc et al. As mentioned by Toublanc et al., this is most probably a consequence of their more detailed treatment of the light propagation. However, it is difficult to really assess the importance of this difference on the overall results of the photochemical model.

5.2. Sensitivity of Vertical Distributions to Eddy Diffusion Profile

Approach. An important step in our work is the choice of an eddy diffusion profile, which we select on the basis of a number of preliminary tests. Using as a starting point the eddy K profiles of *Strobel et al.* [1992], *Toublanc et al.* [1995], and T. Hidayat et al. (submitted paper, 1996), we computed the vertical profiles of the following species: CH_4, C_2H_2, C_2H_4, C_2H_6, C_3H_8, C_4H_2, CH_3C_2H, and HCN, and compared them with observational determinations. At this point, we did not use as further constraints other nitriles (HC_3N, CH_3CN, and C_2N_2, for which the chemistry is more uncertain), CO (which always appears to be uniformly mixed in the model at the mixing ratio specified at the lower boundary), or CO_2 (whose calculated abundance depends on the assumed external flux of water). For CH_4 the observational constraint was a mixing ratio of $8 \pm 3\%$ at 1125 km [*Smith et al.*, 1982], $6 \pm 1\%$ at 1000 km, and $20 \pm 2\%$ at 1400 km [*Strobel et al.*, 1992]. For all other hydrocarbons, we used the mixing ratios derived from the Voyager/IRIS spectra by *Coustenis et al.* [1989] for the equatorial region. The weighting functions (WFs) calculated by *Coustenis et al.* [1989] indicate that in the case of C_2H_6 and C_2H_2, these mixing ratios pertain to a layer centered near 130 km (4 mbar) and extending (half maximum of the WF) from 85 km (15 mbar) to 200 km (0.8 mbar). For C_2H_4, CH_3C_2H, and C_4H_2 the maximum of the WF occurs at 125, 105, and 110 km, respectively. We therefore essentially compared the mixing ratios predicted by our model at these WF peak altitudes with the values of *Coustenis et al.* [1989]. We note, however, that Coustenis et al. assumed uniform distributions of the minor species above their condensation level. This is certainly a reasonable starting point, but we find mixing ratios which vary by 1 or more order(s) of magnitude across the sounded altitude range, as defined by the width of the WFs. Therefore, while the simple comparison of the mixing ratio at the central altitude can give us a feeling of whether our distributions are adequate or not overall, a definite test of the modeling would require us to compute synthetic spectra based on our calculated mixing profiles and check them against the IRIS data. We note that vertical information is available for some compounds in the north polar region [*Coustenis et al.*, 1991]. However, our model is not adapted to high latitudes. The enhanced abundances of some compounds in the polar region compared to the equatorial values are probably at least partly due to the fact that the north pole was in the shadow during the Voyager encounter, implying a reduced photolytical destruction of these species

Table 4. Results of the Model for the Different Eddy K Profiles

Species	Altitude	Observed Value	K_S	K_{Hidayat}	K_{Tanguy}	K_{Tanguy}[a]	Nominal K
CH_4	40	(0.5–4.4)%	3%[a]	3%[a]	3%[a]	1.5%[a]	1.7%[a]
	1000	(6 ± 1)%	4.3%	3.8%	13%	5.1%	4.7%
	1125	(8 ± 3)%	6.1%	6.7%	23%	9.5%	8.6%
	1400	(20 ± 2)%	16%	22%	53%	29%	26%
C_2H_2	>825	~1–2%	0.03%	0.01%	0.25%	0.2%	0.1%
	~725	~0.1–0.3%	0.02%	0.002%	0.02%	0.1%	0.07%
	130	$(2.2^{+0.7}_{-0.9}) \times 10^{-6}$	9.4 (−7)	9.1 (−7)	5.5 (−6)	3.6 (−6)	3.0 (−6)
C_2H_6	130	$(1.3^{+0.2}_{-0.7}) \times 10^{-5}$	1.7 (−6)	1.8 (−6)	1.9 (−5)	1.5 (−5)	8.7 (−6)
C_2H_4	125	$(9^{+3}_{-5}) \times 10^{-8}$	6.7 (−8)	2.9 (−8)	8.5 (−8)	7.5 (−8)	8.3 (−8)
CH_3C_2H	105	$(4.4^{+1.7}_{-2.1}) \times 10^{-9}$	5.0 (−12)	3.0 (−11)	2.4 (−11)	1.0 (−11)	2.3 (−11)
C_3H_8	125	$(7 \pm 4) \times 10^{-7}$	3.0 (−9)	6.0 (−9)	2.7 (7)	2.8 (−7)	1.0 (−7)
C_4H_2	110	$(1.4^{+0.6}_{-0.7}) \times 10^{-9}$	1.6 (−11)	1.3 (−11)	6.4 (−9)	6.5 (−9)	4.7 (−9)
HCN	110	$(1.6^{+0.4}_{-0.6}) \times 10^{-7}$	2.4 (8)	5.0 (−8)	1.1 (−7)	1.4 (−7)	1.2 (−7)
	170	3.3×10^{-7}[b]/2×10^{-7}[c]	1.2 (−7)	2.2 (−7)	6.3 (−7)	7.5 (−7)	6.2 (−7)
	300	5.0×10^{-6}[b]/4×10^{-7}[c]	2.5 (−6)	1.0 (−6)	1.1 (−5)	8.7 (−6)	6.4 (−6)

Read 9.4(−7) as 9.4×10^{-7}.
[a]assumed at the lower boundary (40 km).
[b]*Tanguy et al.* [1990].
[c]T. Hidayat et al. (submitted paper, 1996).

[*Yung*, 1987]. These effects can be properly modeled only with a detailed geometric treatment and a time-dependent code. For HCN we used the equatorial mixing ratio at 110 km inferred from the IRIS spectra [*Coustenis et al.*, 1989] and the vertical distribution at 170–300 km determined for millimeter-wave observations [*Tanguy et al.*, 1990; T. Hidayat et al., submitted paper, 1996]. We note that these two distributions are marginally inconsistent with each other, with the HCN profile of Tanguy et al. increasing much faster above 200 km than that of Hidayat et al.

Test results and the proposed K profile. Results of the calculations with several possible profiles of the eddy diffusion coefficient are given in Table 4. We start with the eddy profile of *Strobel et al.* [1992] and a tropopause CH_4 mixing ratio of 3%. These conditions are therefore meant to reproduce the Strobel et al. calculations of the CH_4 thermospheric profile, and our results on CH_4 are, overall, consistent with theirs, although we tend to find slightly lower CH_4 mixing ratios. (The difference probably comes from the fact that Strobel et al. used a formulation based on the earlier analysis of *Steiner and Bauer* [1990], who assumed conservation of the methane flux in the atmospheric region of interest, i.e., that the methane photolysis occurs entirely above the upper boundary of the model. In fact, significant methane photolysis occurs down to 700 km, an aspect handled by our model but not by the models of *Steiner and Bauer* [1990] and *Strobel et al.* [1992].) However, we find that with this profile of K, it is impossible to fit the observed hydrocarbon abundances, as all predicted abundances are too low. In particular, the calculated C_2H_2, C_2H_6, and C_4H_2 mixing ratios fall short by factors of 2.3, 7.5, and 100, respectively. In contrast, the HCN profile is somewhat lower but reasonably consistent with the retrieval of *Tanguy et al.* [1990].

Tests with the K profile of T. Hidayat et al. (submitted paper, 1996), extrapolated above 400 km in the manner described in section 4, lead to essentially the same results. The CH_4 thermospheric profile is in good agreement with the observations, and as expected, the HCN profile approximately matches the distribution inferred by Hidayat et al. However, this profile provides a fit of the C_2 hydrocarbons as poor as (if not worse than) the Strobel et al. profile. In addition to the shortcomings of the Strobel et al. profile, the ethylene mixing ratio is no longer reproduced.

Calculations with the eddy profile proposed by Toublanc et al. (and keeping a CH_4 stratospheric mixing ratio of 3%) give very different results. Because K in this model is much lower than in the previous ones, most mixing ratios significantly increase. As a result, several important hydrocarbons are decently fit in the lower stratosphere, notably C_2H_6, C_2H_4, and C_3H_8. However, the mixing ratios of a number of other hydrocarbons are now overpredicted. This is notably the case for C_2H_2 (by a factor of 2.5) and C_4H_2 (by a factor of 5). Perhaps even more important, the CH_4 thermospheric mixing ratio is too large by a factor more than 2 at 1000–1400 km. Finally, the HCN mixing ratio is in satisfactory agreement with observations at 110 km but increases too fast above this altitude, and is in only marginal agreement even with the distribution of *Tanguy et al.* [1990].

These tests suggest that (1) if a CH_4 mixing ratio of 3% is adopted in the lower stratosphere, it is difficult to reproduce at the same time the CH_4 thermospheric profile and the C_2 hydrocarbons stratospheric abundance, and (2) K profiles that allow a satisfactory fit of the HCN distribution underpredict the hydrocarbons. In an attempt to fix these problems, we investigated models with a lower CH_4 stratospheric abundance (as mentioned previously, the CH_4 mixing ratio in the lower stratosphere is not well determined). Specifically, we reran our code with the K profile of *Toublanc et al.* [1995], but with CH_4 = 1.5% at the lower boundary. This case, which in principle, mimicks the calculations of *Toublanc et al.* [1995], allows a significant improvement, as CH_4, C_2H_2, C_2H_6, C_2H_4, and C_3H_8 are reasonably well reproduced. However, C_4H_2 is still overpredicted by a factor of 5, and HCN is still somewhat too large at 170 km and above. The CH_3C_2H mixing ratio is also dramatically too low (factor of 400). This latter, serious, problem is probably due to some missing or wrong chemical reaction, or to an incorrect treatment of the CH_3C_2H photolysis, as we were never able to significantly modify the CH_3C_2H mixing ratio by playing with the K profiles (see below).

We attempted to improve the fit for C_4H_2 and HCN (i.e., to decrease them) by finetuning the K profile and the CH_4 mixing

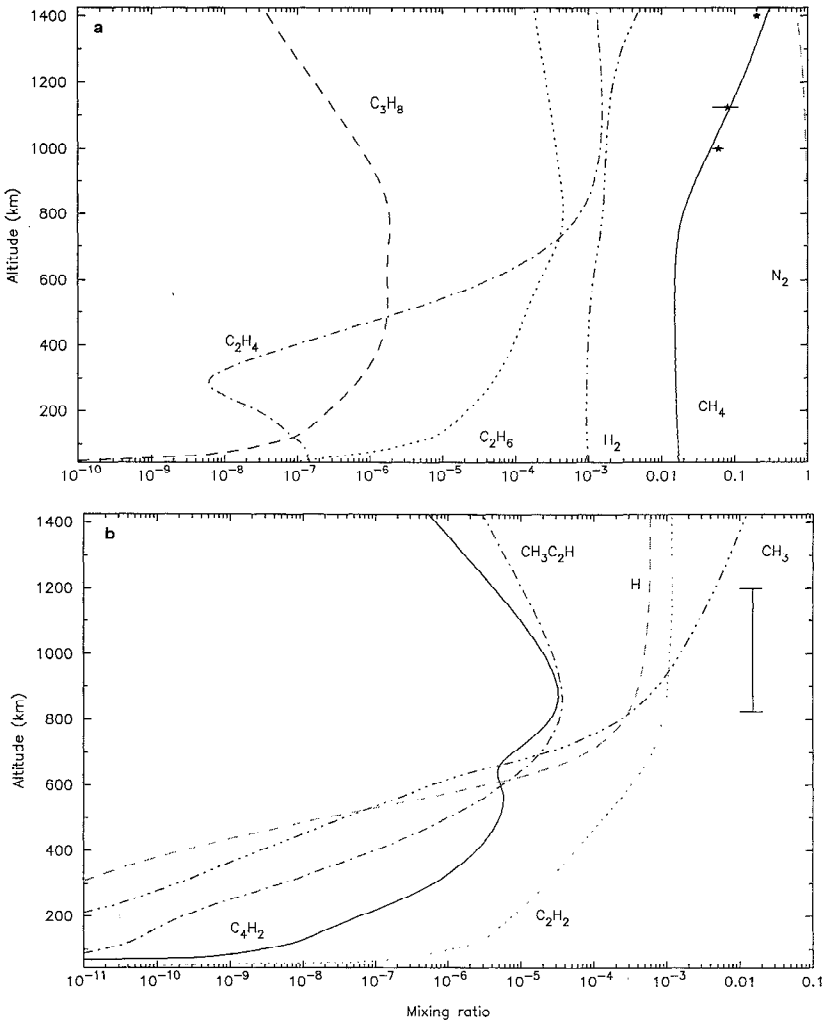

Figure 5. Altitude mixing ratio profiles of hydrocarbons. (a) Stars and associated error bars represent the observed thermospheric profile of CH_4. (b) Vertical solid line represents the estimated thermospheric (at $z >$ 825 km) C_2H_2 mixing ratio from Voyager/UVS [*Smith et al.*, 1982].

ratio at the lower boundary. We tested a K profile intermediate between those of Toublanc et al. (K_T) and Strobel et al. (K_S), defined as $K_N = (K_T^2 K_S)^{1/3}$, and assumed in this case CH_4 = 1.7%. As is clear from Table 4, this attempt was not really successful. Only a slight improvement was obtained on C_4H_2 and HCN (and on C_2H_2 as well), and the price to pay was a significant degradation on C_3H_8. We therefore regard the two cases as providing similar fits to the overall chemistry and we use the last case (K_N, and CH_4 = 1.7%) as the nominal one. We stress that neither of these cases allows us to fit the HCN distribution of T. Hidayat et al. (submitted paper, 1996). Fitting hydrocarbons and HCN simultaneously with the current chemistry and simple K profiles seems difficult. One possibility to solve the dilemma would be to invoke more complex profiles of K (e.g., with discontinuities with altitude). Another explanation would be that a large loss of HCN is omitted in the model. Based on a haze material production rate determined from microphysical models, and assuming a typical C:N rate of 4:1 in the haze (based on laboratory measurements on tholins), *McKay* [1996] has recently estimated that the production of Titan's haze represents a loss rate of N atoms of about 10^8 cm^{-2} s^{-1}. This is comparable to the net HCN production rate (see below). Therefore if the haze is produced through HCN polymerization, then the haze formation represents a major sink for HCN. Future photochemical models should consider this possibility seriously.

6. Discussion

6.1. Hydrocarbons

The hydrocarbon profiles are shown in Figures 5 and 6 for our nominal K profile. In Table 5 we give the integrated production and loss rates for all species in the model (all fluxes and integrated rates are referred to the tropopause). For a number of species whose fate after their production is not followed in the model, we also give the production rate. For the condensing species, we also give the condensation rates, as calculated from (6) and (7). It can be verified that satisfactory convergence is achieved by the model. For most species of Table 5 the calculated condensation rates agree reasonably well with the integrated difference between production and loss. The only significant discrepancies are for ethane, methylacetylene, and water. It turns out that for these species, the supersaturation (essentially proportional to the ratio of the net

loss rate to the vapor pressure at the condensation level) is particularly low (about 10^{-6}). In this case, as mentioned in section 3.5, a convergence criterion of 1 part in 10^4 is not sufficient to accurately calculate the supersaturation. In all cases the values given in the $P - L$ column must be preferred for controlling the mass conservation. The carbon net loss rate from CH_4 is 8.0×10^9 cm^{-2} s^{-1}, and the total condensation rate of carbon (calculated from $P - L$) in C_2H_6 and C_2H_2 is $2 \times (2.62 + 0.94) \times 10^9 = 7.1 \times 10^9$ cm^{-2} s^{-1}, i.e., 10% less than the preceding value. Condensation of C_3H_8 and C_4H_2 and production of heavier hydrocarbons (in particular, C_6H_2) accounts for the difference.

Taking for the troposphere the nominal model of *Yelle et al.* [1996], the total CH_4 column density is about 7×10^{24} molecules cm^{-2}. With our CH_4 net destruction rate, the lifetime for CH_4 is 28 m.y. Our CH_4 loss rate is comparable, though slightly smaller, than previous estimates by *Yung et al.* [1984] and *Toublanc et al.* [1995] (1.5 and 1.3×10^{10} cm^{-2} s^{-1}, respectively). Consistent with these earlier studies, we find that 27% of the CH_4 destruction rate is due to direct photolysis, while catalytic cycles account for the remaining 73%. The short lifetime of methane is the main requisite for the existence of a methane source at Titan's surface, either in the form of oceanic/lake supply or through episodic volcanism (see review by *Lunine* [1995]).

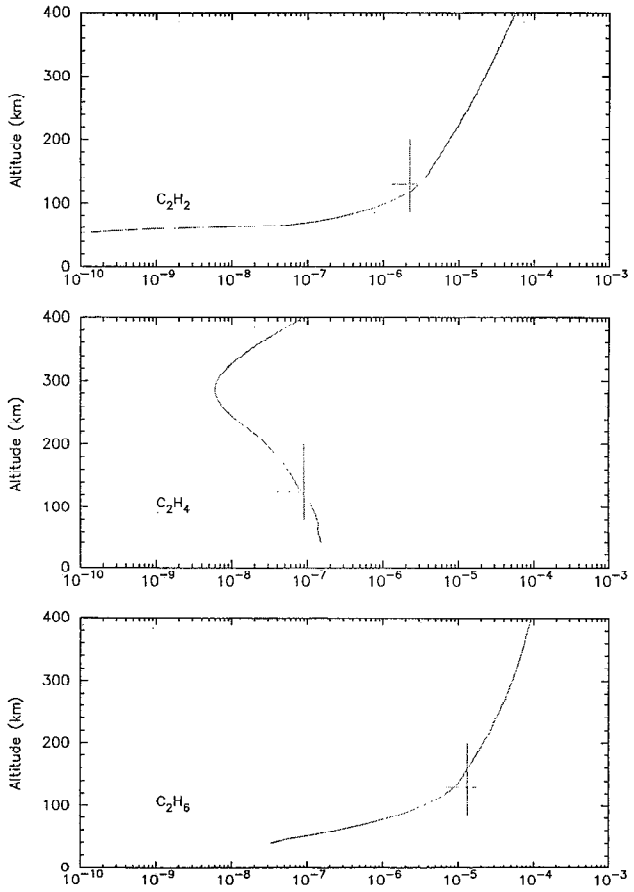

Figure 6a. Stratospheric mixing ratio profiles of C_2H_2, C_2H_4, and C_2H_6. The error bars give the range of measured mixing ratios from Voyager/IRIS equatorial spectra [*Coustenis et al.*, 1989]. The vertical error bars cover the altitude range in which the weighting function is at least equal to its value at half-maximum (see text).

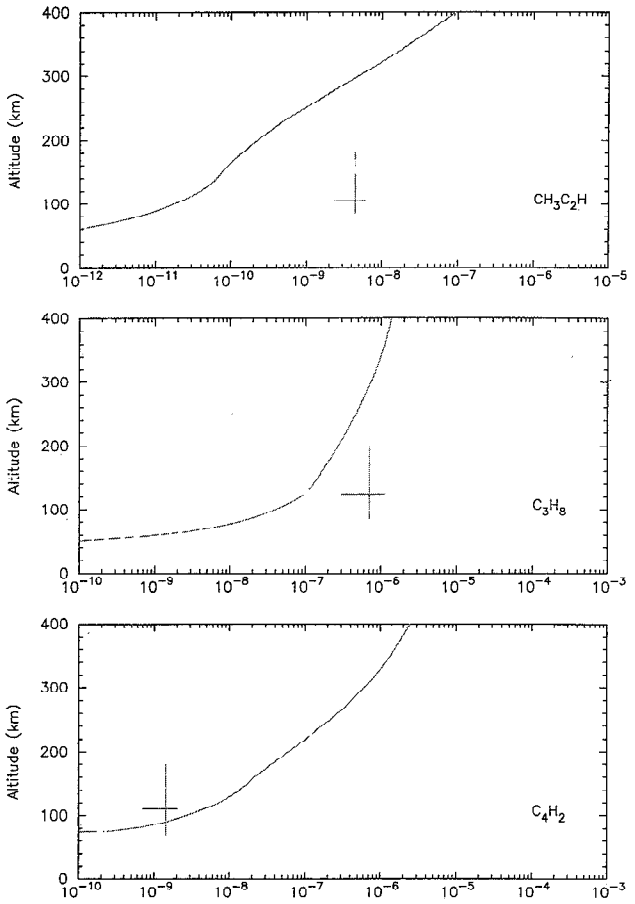

Figure 6b. Same as Figure 6a for CH_3C_2H, C_3H_8, and C_4H_2.

The loss rate of CH_4 liberates 3.2×10^{10} H atoms cm^{-2} s^{-1}. Condensation of C_2H_6, C_2H_2, and C_3H_8 consumes 1.9×10^{10} cm^{-2} s^{-1}, and the remaining 1.3×10^{10} cm^{-2} s^{-1} are lost through escape of H (2.4×10^9 cm^{-2} s^{-1}) and H_2 ($2 \times 5.2 \times 10^9$ cm^{-2} s^{-1}). Our H atom flux is somewhat smaller than that given by *Toublanc et al.* [1995] (6.5×10^9 cm^{-2} s^{-1}) and provides a better match of the value inferred from a model of Titan's hydrogen torus, (1–3) $\times 10^9$ cm^{-2} s^{-1} [*Smyth*, 1981]. Our H_2 escape rate is also ~2 times smaller than that of *Toublanc et al.* [1995].

The acetylene and ethane stratospheric mixing ratios in our nominal model fall within the error bars of *Coustenis et al.* [1989] (Figure 6a). One may note, however, that we tend to overestimate the C_2H_2/C_2H_6 ratio (0.35 versus an observed value of $0.17^{+0.31}_{-0.11}$). The C_2H_2/C_2H_6 ratio is a problem often encountered by photochemical models. In the case of Neptune, *Romani et al.* [1993] were able to reproduce the observed value only by making use of a K profile sharply varying with altitude, with a region of stagnancy at 1–100 mbar and a region of fast mixing at upper levels. The most serious problem with acetylene is the fact that the computed thermospheric C_2H_2 mixing ratio, 0.1% at 1125 km, markedly conflicts the UVS-derived value (1–2%) at $z > 825$ km. This problem has been encountered earlier [*Yung et al.*, 1984; *Toublanc et al.*, 1995], and the favorite explanation has been that the opacity attributed to C_2H_2 in the UVS curves may have been caused by other mol-

Table 5. Column-Integrated Rates for the Compounds Considered in the Model

Species	Production P	Loss L	$P - L$	Condensation Flux Φ_c From (6) and (7)
CH_4	4.44×10^7	8.01×10^9	-7.97×10^9	
CH_3	6.00×10^9	6.01×10^9	-3.60×10^6	
C_2H_2	5.18×10^9	4.24×10^9	9.39×10^8	9.28×10^8
C_2H_4	1.20×10^9	1.24×10^9	-3.46×10^7	
C_2H_6	2.75×10^9	1.22×10^8	2.62×10^9	1.41×10^9
CH_3C_2H	7.17×10^7	7.13×10^7	3.64×10^5	1.13×10^4
C_3H_8	3.79×10^7	5.49×10^6	3.23×10^7	3.14×10^7
C_4H_2	5.80×10^{10}	5.80×10^{10}	2.80×10^6	2.27×10^6
H	6.83×10^9	4.44×10^9	2.39×10^9	
H_2	5.23×10^9	1.13×10^6	5.23×10^9	
CH_2CCH_2	8.17×10^3			
C_3H_6	4.51×10^6			
C_3H_7	3.27×10^6			
C_4H_6	2.00×10^6			
C_4H_8	2.25×10^6			
C_4H_{10}	6.55×10^6			
C_6H_2	4.79×10^7			
C_8H_2	9.21×10^6			
CO	1.10×10^7	1.27×10^7	-1.67×10^6	
CO_2	4.11×10^6	2.22×10^5	3.89×10^6	3.81×10^6
HCO	8.77×10^6	8.77×10^6	3.72×10^1	
$O(^3P)$	2.91×10^5	3.06×10^5	-1.46×10^4	
H_2O	6.69×10^6	6.62×10^6	6.47×10^4	3.70×10^4
HCN	3.17×10^9	3.08×10^9	9.10×10^7	8.00×10^7
HC_3N	2.39×10^8	2.36×10^8	3.73×10^7	3.73×10^7
C_2N_2	1.48×10^5	1.44×10^5	3.64×10^4	2.89×10^4
C_4N_2	3.08×10^7	3.07×10^7	1.33×10^5	7.20×10^6
CH_3CN	6.91×10^5	3.20×10^4	6.59×10^5	6.61×10^5
$N(^4S)$	7.44×10^8	7.44×10^8	-6.76×10^5	
N_2	2.11×10^8	7.79×10^8	-5.67×10^8	
Products (R91)	1.62×10^7			
Products (R92)	3.02×10^7			
CH_2NH	5.40×10^8			
C_2H_3CN (R96)	3.18×10^8			
C_2H_3CN (R104)	1.44×10^7			
CH_2CN	2.56×10^4			

Values are in units of $cm^{-2}\ s^{-1}$.

ecules. This explanation seems plausible, but no single species has been proposed. In particular, HCN, the only molecule (besides N_2 and CH_4) with an abundance comparable to C_2H_2, does not absorb significantly at the relevant wavelengths ($\sigma_{C_2H_2}/\sigma_{HCN} = 70$ and 5 at 130 and 155.5 nm, respectively).

Our nominal model overpredicts the C_4H_2 mixing ratio by a factor of 3.5 and underpredicts C_3H_8 by a factor of 7 ± 4 (Figure 6b). However, we do not feel this necessarily indicates errors in the adopted chemistry because these two species appear to be very sensitive to the eddy K profile. Specifically, if we use the eddy profile of *Toublanc et al.* [1995], and a CH_4 stratospheric mixing ratio of 1.5%, the C_3H_8 abundance becomes marginally consistent with the observations. In addition, calculations with the eddy K profile of *Strobel et al.* [1992] and T. Hidayat et al. (submitted paper, 1996) underpredict C_4H_2. Therefore it might be possible to get these two species in better agreement with observations by investigating more complicated eddy diffusion profiles.

The most serious shortcoming of our model is its failure to reproduce the CH_3C_2H abundance. In all our investigated cases, the calculated CH_3C_2H mixing ratio is $(0.5–2) \times 10^{-11}$, i.e., 250–1000 times lower than observed (Figure 6b). *Toublanc et al.* [1995] reach a much better agreement on CH_3C_2H, which they overpredict by a factor of 3 only. We were not able to understand the origin of the huge difference between the two models. For CH_3C_2H, we used a nominal chemistry similar to that of *Yung et al.* [1984]. We attempted to modify a number of relevant reactions and reactions rates according to the model of *Toublanc et al.* [1995], but this led to very small changes in our predictions of CH_3C_2H. On the other hand, it appears that the predicted mixing profile of CH_3C_2H is very sensitive to photolysis. Specifically, if we turn off the CH_3C_2H photolysis, we obtain CH_3C_2H mixing ratios in the range of several 10^{-7} at 100–200 km, now much higher than observed. We have used photolysis cross sections from *Nakayama and Watanabe* [1964] and *Hamai and Hirayama* [1979] and quantum yields from *Yung et al.* [1984].

Finally, we predict significant formation of polyynes (C_6H_2 and C_8H_2), mainly between 300 and 900 km. The integrated production rate of C_6H_2 (see Table 5) corresponds to $\sim 6 \times 10^{-15}$ g $cm^{-2}\ s^{-1}$. This number is similar to the haze production rates inferred from Voyager observations by *McKay et al.* [1989] and *Samuelson and Mayo* [1991]. The production of C_8H_2 is ~5 times lower.

6.2. Nitriles

In Figure 7 we show the HCN profiles calculated using the eddy profiles of *Strobel et al.* [1992], T. Hidayat et al. (submitted paper, 1996), and the nominal case used in this work. These profiles are compared with the observed HCN profiles of *Tanguy et al.* [1990] and T. Hidayat et al. (submitted paper, 1996). Reassuringly, the HCN distribution calculated with the eddy

profile of Hidayat et al. matches reasonably well their observed profile, with however, some difference above 200 km, where our HCN profile increases somewhat too much with respect to the observations. As mentioned previously, our nominal model does not allow a good fit of the HCN distribution.

With our nominal model, the net production of N atoms from the photolysis and the GCR impact of N_2 is 1.1×10^9 cm^{-2} s^{-1} (Table 5). Condensation of HCN consumes only 10% of these atoms (0.9×10^8 cm^{-2} s^{-1}). This result is consistent with *Toublanc et al.* [1995], who obtain a net production of HCN of $(0.5–1) \times 10^8$ cm^{-2} s^{-1} for a total N production of 8.4×10^8 cm^{-2} s^{-1}. Condensation of HC_3N in this model accounts for a loss of 3.7×10^7 cm^{-2} s^{-1} N atoms, but this number (and the condensation fluxes of C_2N_2, CH_3CN, and C_4N_2 as well) may be overestimated because our nominal model overpredicts all nitriles (see below). In the model, most of the N atoms liberated from the N_2 destruction end up in compounds whose fate after their production is not followed, the most important of which are CH_2NH and C_2H_3CN, whose summed production is equivalent to 8.7×10^8 cm^{-2} s^{-1}. The CH_2NH (methylenimine) production, due to the reaction between CH_3 and NH (itself generated in reactions between $N(^2D)$ and H or CH_3) is ~6 times lower than the HCN production and 6 times larger than the HCN net condensation rate. This result is in essence similar to that obtained by *Lellouch et al.* [1994], who modeled the HCN formation at Neptune and found that, for a source of atomic nitrogen provided by GCR impact on internal N_2, the production of CH_2NH was comparable to the net HCN production rate. These considerations have led one of us (E.L.) and colleagues to search for CH_2NH in Titan's atmosphere at millimeter wavelengths. Observations were unsuccessful, however, and it may be presumed that CH_2NH is significantly lost by photolysis and/or condensation.

Similar numbers are found for the various fluxes when running the model with the eddy K profile of T. Hidayat et al. (submitted paper, 1996), except that the HC_3N, C_2N_2, and C_4N_2 condensation fluxes are significantly smaller. These condensation fluxes, however, contribute very little to the overall N balance.

Cyanoacetylene was identified in the Voyager/IRIS spectra of the north polar regions, with a mixing ratio increasing from $8.4^{+3}_{-3.5} \times 10^{-8}$ at 1.5 mbar (170 km), to $2.5 \pm 1 \times 10^{-7}$ at 0.1 mbar (300 km) [*Coustenis et al.*, 1991]. It was not observed in the equatorial spectra, with a typical upper limit of 1.5×10^{-9} at 105 km [*Coustenis et al.*, 1989]. HC_3N was, however, detected from ground-based millimeter-wave observations [*Bézard et al.*, 1992]. The line shape indicated a HC_3N vertical profile strongly increasing with altitude, with a mixing ratio less than 10^{-9} at 200 km and a column density of 1.0×10^{14} cm^{-2} above 320 km. Since these observations primarily sample low and middle latitudes, we take the inferred distribution as representative of equatorial conditions and use them as the primary constraint to our model. The HC_3N profile calculated with three different profiles of K ($K_{Strobel}$, $K_{Hidayat}$, and the K proposed in this work) is shown in Figure 8. In the last case (nominal K), the HC_3N distribution is grossly inadequate, with a mixing ratio $\geq 1.0 \times 10^{-7}$ at 200 km and a column density of 2.7×10^{16} cm^{-2} above 320 km. In the case of the K profile of T. Hidayat et al. (submitted paper, 1996), the upper limit at 200 km is met, but the column density above 320 km is 6 times too small. With the K profile of *Strobel et al.* [1992], we obtain a mixing ratio of 1.3×10^{-9} at 200 km and a column density of 1.3×10^{14} cm^{-2} above 320 km, essentially in agreement with the observations. However, we do not consider our chemical modeling of HC_3N to be satisfactory for the following reason. HC_3N is produced from a number of reactions ((R97), (R102), (R108), (R109)) involving HCN, CN, or C_3N and some hydrocarbons (the most important in our model are $CN + C_2H_2$ and $HCN + C_2H$). As an additional test, we ran the code for the nitriles by using as inputs our nominal K profile and the corresponding hydrocarbon distributions (Figures 5 and 6) and the HCN distribution calculated with the K profile of T. Hidayat et al. (submitted paper, 1996) (solid line of Figure 7). The HCN distribution was held fixed for this test. Although these input conditions are not self-consistent (since the adopted HCN distribution is incompatible with the adopted K profile), this approach provides a good basis from which to investigate the chemistry forming HC_3N. In this case the resulting HC_3N mixing profile in the lower stratosphere remained too high compared with observations (case labeled Test in Figure 8). In other words, even if we start with adequate (i.e., matching the observations) hydrocarbon and HCN profiles, we are unable to correctly reproduce the HC_3N profiles. A possible reason could be that the HC_3N photolysis rate is underestimated in our model. We have used absorption cross sections from *Connors et al.* [1974] and *Bruston et al.* [1989] and efficiencies estimated by analogy with C_2H_2. New (lower) values for the efficiencies have been suggested recently by *Clarke and Ferris* [1995]. Using these new values would only exacerbate the problem.

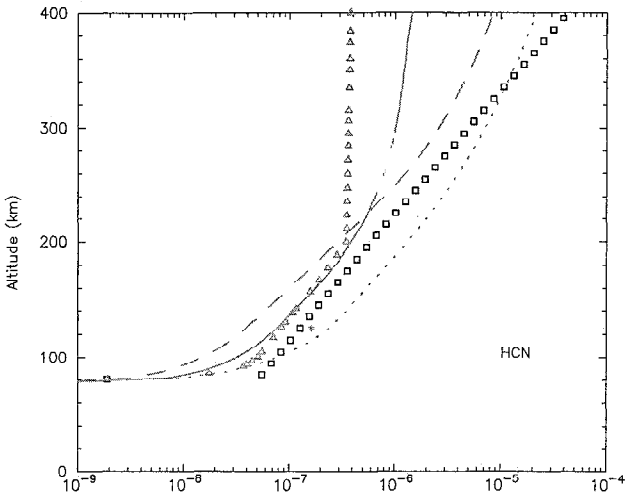

Figure 7. Stratospheric mixing ratio profile for HCN. Symbols show the observations, and lines show the models. Open squares, *Tanguy et al.* [1990]; triangles, T. Hidayat et al. (submitted paper, 1996); star, Voyager/IRIS measurement [*Coustenis et al.*, 1989]; solid line, HCN profile computed with the eddy K profile of Hidayat et al.; dashed line, same with the eddy K profile of *Strobel et al.* [1992]; dotted line, same with the eddy K profile proposed in this work and allowing the best match to hydrocarbons.

Figure 9 shows the calculated profiles for C_2N_2 and C_4N_2, calculated with the K profile of Hidayat et al. and our nominal K profile. Observational constraints on these two compounds are scarce. None was detected by Voyager at equatorial latitudes, and the only information is an upper limit on the C_2N_2 mixing ratio of 1.5×10^{-9} [*Coustenis et al.*, 1989]. In the polar regions, C_2N_2 was observed with a mixing ratio of about $5.0 \times$

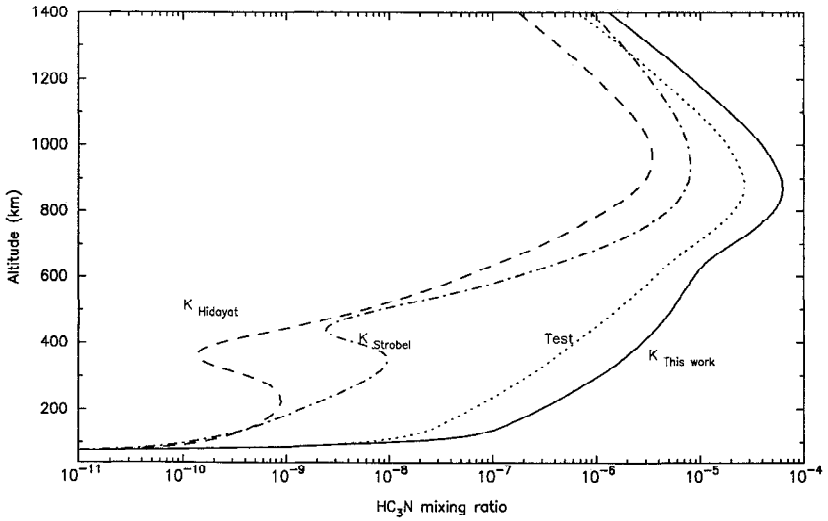

Figure 8. Altitude mixing ratio profiles of HC_3N for various choices of the eddy K profile. See text for description of profile labeled Test.

10^{-9} at 170 mbar and 2.0×10^{-8} at 300 km, and C_4N_2 was identified in its solid phase [*Hanel et al.*, 1981]. All of our models easily match the upper limit on equatorial C_2N_2, with predicted mixing ratios of 10^{-12} to 10^{-11} at 170 km. Consistent with *Yung* [1987], we predict larger mixing ratios for C_4N_2 than for C_2N_2. Unfortunately, no direct observational constraints on C_4N_2 are available.

Ground-based millimeter-wave observations have also permitted the detection of acetonitrile [*Bézard et al.*, 1993]. The retrieved mixing profile increases from 1.5×10^{-9} at 180 km to 3.5×10^{-9} at 250 km and 1.0×10^{-8} at 320 km. As we mentioned in section 3, CH_3CN can plausibly be formed by reactions between CH_4 and CN, or between C_2H_6 and CN. These two reactions mostly produce HCN, but could also give CH_3CN with a small quantum yield. We studied these two mechanisms separately. Specifically, in each of the two cases, we adjusted the quantum yield in order to match the observed CH_3CN column abundance and compared each time the vertical distribution with the observations. For this exercise, we adopted the same approach as for the test on HC_3N previously described, so as to start with realistic CH_4, C_2H_6, and HCN (and hence CN) distributions. Results are shown in Figure 10. The required quantum yield is 5% for CH_4 + CN and 3.5% for C_2H_6 + CN, which is probably not unreasonable. The two vertical distributions are similar below 280 km, where they provide an overall acceptable match to the observed CH_3CN profile. Above this altitude, the calculations tend to underestimate the increase of CH_3CN with altitude, particularly in the CH_4 + CN case. *Bézard et al.* [1993] performed the same analysis in a somewhat improved way, by generating synthetic spectra based on their photochemical distribution for CH_3CN and testing them against the data. They obtained similar quantum yields to ours and found that only the C_2H_6 + CN hypothesis provided a satisfactory vertical distribution of CH_3CN. Our calculations also tend to favor this production mechanism. However, reaching more definite conclusions on this matter (as well as on the main loss processes for CH_3CN; we here include only photolysis and condensation) will first require that we are able to model the HCN and hydrocarbons self-consistently. Of course, laboratory measurements on the

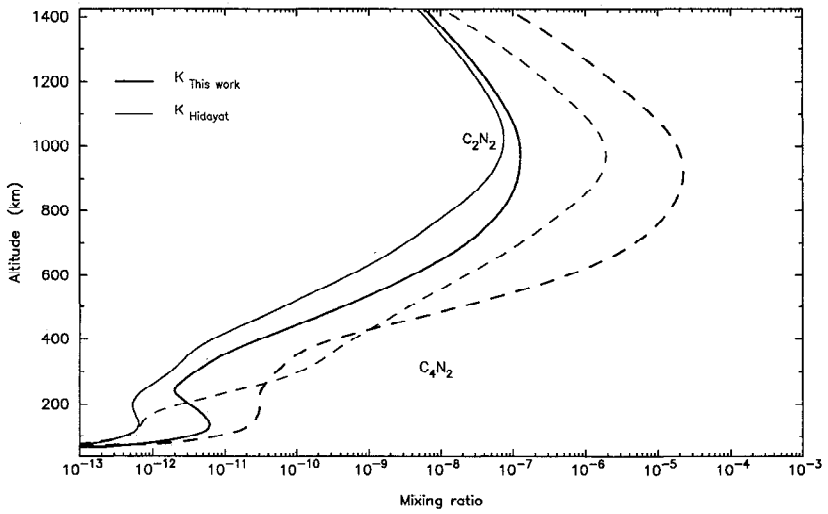

Figure 9. Altitude mixing ratio profiles for C_2N_2 (solid lines) and C_4N_2 (dashed lines).

paths and relative yields of the CH_4 + CN and C_2H_6 + CN reactions are also necessary to settle this issue.

6.3. Oxygen Compounds

Only two oxygen-bearing compounds have been detected in Titan's atmosphere, namely, CO_2 and CO. Preliminary analyses of the Voyager/IRIS spectra indicated a stratospheric abundance of about 1.5×10^{-9}, representing the CO_2 average mole fraction above the 110-mbar level [*Samuelson et al.*, 1983]. The more recent analysis of *Coustenis et al.* [1989], assuming a vertically uniform distribution of CO_2, suggests a mixing ratio of $1.4^{+0.3}_{-0.5} \times 10^{-8}$, representative of the 110- to 130-km altitude region. However, *Coustenis et al.* [1989] also tested a more realistic, altitude-varying distribution adapted from *Samuelson et al.* [1983]. We use this distribution as a test of our model. The case for CO is controversial, as successive millimeter-wave observations have led to divergent results as to the CO stratospheric abundance [*Muhleman et al.*, 1984; *Paubert et al.*, 1984; *Marten et al.*, 1988; *Gurwell and Muhleman*, 1995]. Since photochemical models normally predict a uniformly mixed CO throughout the atmosphere, we adopt here the *Gurwell and Muhleman* [1995] nominal stratospheric abundance of 5.0×10^{-5} because it is the one that gives the best agreement with the CO tropospheric mixing ratio, as determined by *Lutz et al.* [1983]. We note, however, that this may not be the final word, as such a uniform profile is in contradiction to the recent observations of several CO rotational lines by *Hidayat et al.* [1995]. In addition, from an analysis of the 4.7-μm window in Titan's spectrum, K. S. Noll et al. (Titan's 5 μm spectral window: Carbon monoxide and the albedo of the surface, submitted to *Icarus*, 1996; hereinafter referred to as submitted paper) very recently inferred a CO mixing ratio of 10^{+10}_{-5} ppm at tropospheric levels.

In the absence of any external source of water, the production of CO_2 is so small that the computed CO_2 stratospheric mixing ratio remains determined by the saturation value (Figure 11). Assuming a CO mixing ratio of 5×10^{-5} at the lower boundary, we also show in Figure 11 the CO_2 distribution for the water ablation profile shown in Figure 1, and for 2 and 3 times this reference profile. Though not strictly parallel, the calculated profiles are similar to the profile used by Coustenis et al. It would be useful to test our CO_2 distributions directly against the IRIS spectra, but we provisionally regard the case with 2 times the reference ablation profile of Figure 1 as providing the best overall match. In this case, which corresponds to an integrated H_2O ablation rate of 6.2×10^6 cm^{-2} s^{-1}, the condensation flux for CO_2 is 3.9×10^6 cm^{-2} s^{-1}, and the conservation of O atoms is achieved through an upward flux of CO of about 1.6×10^6 cm^{-2} s^{-1} at the lower boundary. Thus CO is not in equilibrium, as its loss rate is slightly larger than its production rate (by 15%). A continuous supply of CO of 1.6×10^6 cm^{-2} s^{-1} over 4.55 b.y. represents about 2.0×10^{23} molecules cm^{-2}. With a CO mixing ratio of 5×10^{-5}, corresponding to a column density of 1.0×10^{22} cm^{-2}, this supply is equivalent to 20 times the atmospheric inventory. We feel that this situation is unlikely, at least for an oceanic reservoir, because even a global, methane-rich ocean at 101 K (the largest possible CO oceanic reservoir) would be able to hold only 11 times the atmospheric inventory [*Dubouloz et al.*, 1989]. The possibility of other (volcanic) supply of CO may remain, but we feel that it is important to investigate alternative situations as well. For CO to be in equilibrium (integrated $P = L$), we find that the CO mixing ratio must be equal to 1.0×10^{-3}. This value is smaller than that found by *Samuelson et al.* [1983] and *Yung et al.* [1984] by a factor 10–20, but we note that these authors used an external source of oxygen (6.1×10^5 cm^{-2} s^{-1}) essentially 10 times lower than that in our model, resulting in lower OH abundances. A CO mixing ratio of 1.0×10^{-5} is outside the error bars of *Gurwell and Muhleman* [1995]. It would be more in line with the stratospheric mixing ratios reported recently by *Hidayat et al.* [1995], but we hasten to add that our model cannot (and no simple photochemical model can) explain a CO mixing profile decreasing with altitude as does the *Hidayat et al.* [1995] profile. On the

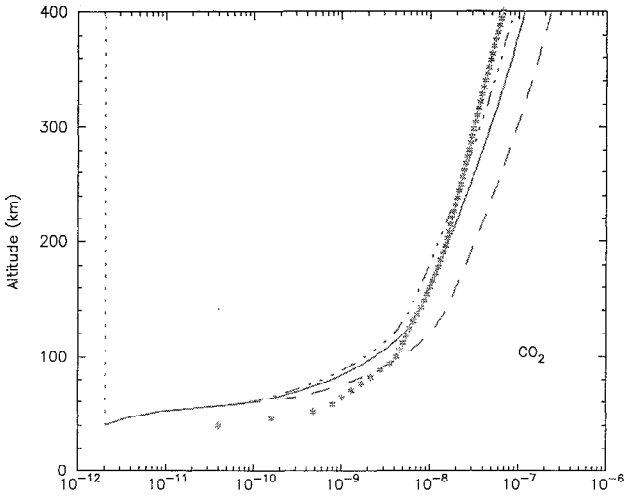

Figure 11. Stratospheric mixing ratio profile for CO_2. Symbols represent a profile fitting the Voyager/IRIS data [*Coustenis et al.*, 1989]. The vertical dotted line is the CO_2 profile calculated in the absence of an external source of oxygen. Dashed-dotted line shows calculated CO_2 profile with the ablation rate of Figure 1, taken from *English et al.* [1996] (see text). Thick solid line shows same, with twice this rate. Dashed line shows same, with 3 times this rate.

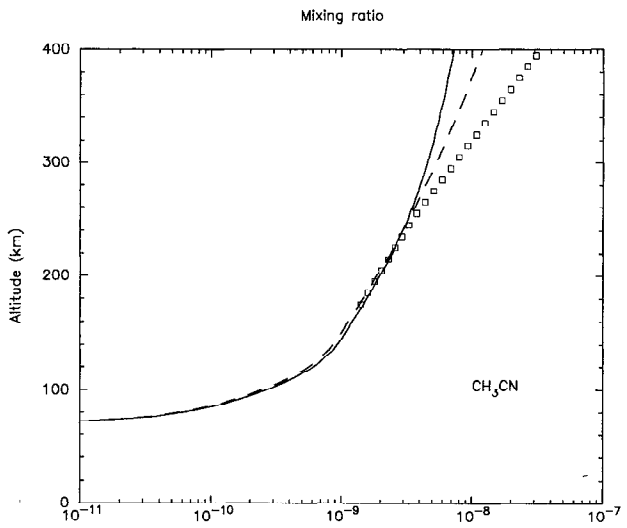

Figure 10. Stratospheric mixing ratio profile for CH_3CN. The open squares show the approximate observed distribution [*Bézard et al.*, 1993]. Solid line shows calculated profile assuming CH_3CN is produced from CN + CH_4. Dashed line shows same, assuming production from CN + C_2H_6.

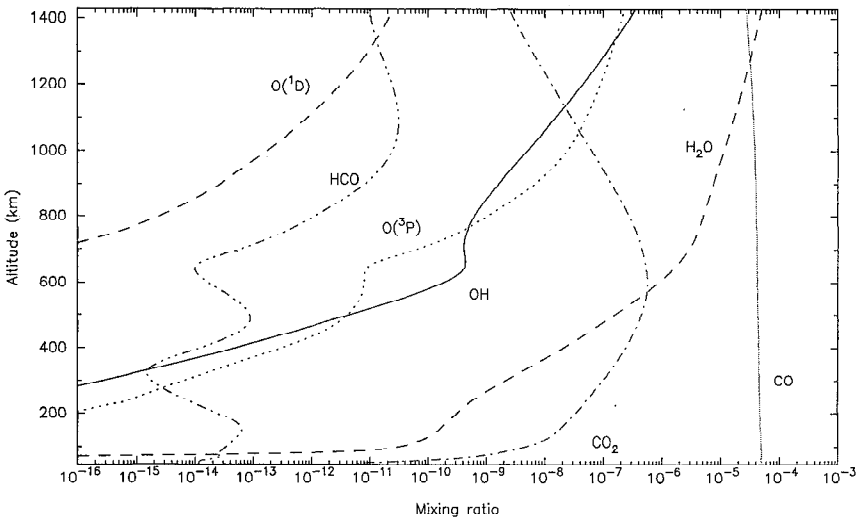

Figure 12. Altitude mixing ratio profile for oxygen compounds.

other hand, such a mixing ratio is fully consistent with the K. S. Noll et al. (submitted paper, 1996) result.

Another alternative is that the meteoritic flux incoming to Titan contains oxygen not only in the form of water ice, but also significant amounts of carbon monoxide. (CO has been detected in distant comets [e.g., *Crovisier et al.*, 1995], and laboratory experiments suggest that, upon warming, H_2O/CO ice mixtures are able to retain CO ice up to ~120 K [e.g., *Sandford and Allamandola*, 1988].) We reran our model with various compositions for the infalling meteoroids and found that reproducing the observed CO_2 profile and a steady state (i.e., zero CO flux at the lower boundary) CO mixing ratio of 5×10^{-5} at Titan can be achieved with an external oxygen flux of 7.8×10^6 cm^{-2} s^{-1} (i.e., 2.5 times the *English et al.* [1996] model) containing 80% H_2O and 20% CO. Although a 20% CO mixing ratio exceeds the estimated CO abundance in comets (about 10%), this calculation shows that a significant fraction of Titan CO may be directly injected from an external source.

An external flux of water 2 times larger than that in the nominal model of *English et al.* [1996] does not seem unreasonable. In this model the largest potential source of error comes from the uncertainty in the particle flux at Titan. Such a flux was estimated from extrapolation of the well-known interplanetary flux at 1 AU through the poorly characterized region of Jupiter and farther on into the essentially unconstrained region beyond Jupiter. In addition, *English et al.* [1996] did not consider sources external to Titan's orbit (Hyperion, Iapetus, and Phoebe). Thus the flux of ice particles within the Saturnian system may well be underestimated. In conclusion, we suggest that the equilibrium value for CO is in the right ballpark of the observed values and that the H_2O external source required to reproduce the observed CO_2 profile is in plausible agreement with the ablation models.

Our calculated water vapor mixing ratio increases from 3×10^{-11} at 100 km to 1.5×10^{-10} at 150 km and 2×10^{-9} at 300 km (Figure 12). The Voyager/IRIS spectra do not provide any constraint on the water profile as the H_2O rotational lines lie mainly longward of 45 μm. We find a very small condensation of water (condensation flux of 7×10^4 cm^{-2} s^{-1}), and we therefore would predict insignificant formation of water clouds. Water ice is tentatively detected by a feature at 220 cm^{-1} in the IRIS spectra of the north polar regions [*Samuelson*, 1995; A. Coustenis, private communication, 1995], but this feature is absent from the IRIS equatorial spectra, consistent with our prediction of very small water condensation.

7. Conclusions

The vertical distributions of Titan's neutral constituents have been calculated by means of a new photochemical model, and compared with observations available to-date. This model makes use of many recently updated chemical reaction rates. Specific features of the model are a realistic treatment of the oxygen source in Titan's atmosphere, based on an ablation model of H_2O; consideration of the N_2 dissociation by galactic cosmic rays; and a sensitivity study of the results to the eddy diffusion coefficient profile. We have limited our investigation to eddy K profiles "smoothly" varying with altitude (i.e., with no discontinuities).

The main conclusions of this work are as follows.

1. It is not possible to simultaneously reproduce the observed abundances of methane in the thermosphere and of the major (C_2) hydrocarbons (ethane, acetylene, ethylene) in the stratosphere if the CH_4 stratospheric abundance is large (~3%). Essentially, the hydrocarbons require low values of the eddy diffusion coefficient, while fitting the thermospheric methane profile with CH_4 = 3% at the tropopause implies high values of K. Current constraints on the CH_4 stratospheric mixing ratio are loose (0.5–4.4%), and an accurate determination should be considered a priority. Such a determination could be obtained from combined measurements of the rotational lines of CH_4 near 110 μm and of the 7.7-μm band, either with the Infrared Space Observatory (ISO) or Cassini/composite infrared spectrometer (CIRS) [*Coustenis et al.*, 1993].

2. Similarly, it does not appear easy to simultaneously fit the vertical profiles of nitriles and of hydrocarbons. The investigation of several eddy K profiles indicates a large sensitivity of most of the minor compounds to this parameter, confirming the importance of vertical transport in Titan's atmosphere. Fitting the vertical distribution of HCN requires an eddy diffusion coefficient at 100–300 km that is 5–20 times larger than that necessary for the hydrocarbons. Including loss of HCN

through polymerization might solve this problem [*McKay*, 1996].

3. Our model is able to reproduce the observed abundances of C_2H_2, C_2H_4, and C_2H_6 at stratospheric levels. The C_4H_2 and C_3H_8 mixing ratios are not fit within the published error bars, but the order of magnitude is reasonable. Finetuning the shape of the eddy K profile in some specific regions might allow a better match of the measurements.

4. Our model severely underestimates the abundance of CH_3C_2H and overpredicts that of HC_3N. In contrast, we can find a plausible scenario for the formation of CH_3CN, involving the reaction of CN with either CH_4 or (preferably) C_2H_6. The predicted abundance for C_2N_2 is several times less than the available upper limit in the equatorial region.

5. The observed CO_2 abundance can be fit with a realistic external source of water originating from meteoritic ablation and corresponding to a column-integrated deposition of about 6×10^6 cm^{-2} s^{-1}. Maintaining CO at a mixing ratio of 5×10^{-5} requires a CO flux from the surface of 1.6×10^6 cm^{-2} s^{-1}. Equilibrium (i.e., zero flux in and out of the atmosphere) for CO is achieved for a mixing ratio only slightly lower (1×10^{-5}).

Acknowledgments. This research was supported by the Spanish Comisión Interministerial de Ciencia y Tecnología under contracts ESP93-0338 and ESP94-0719. We especially thank M. Banaszkiewicz, B. Bézard, E. Chassefière, A. Coustenis, R. Lorenz, C. McKay, P. Romani, P. Ratcliff, and D. F. Strobel for their help in many of the topics covered by this paper, as well as for the clarifying discussions we have had.

References

Allen, M., J. P. Pinto, and Y. L. Yung, Titan: Aerosol photochemistry and variations related to the sunspot cycle, *Astrophys. J., 242*, L125–L128, 1980.

Atreya, S. K., *Atmospheres and Ionospheres of the Outer Planets and Their Satellites*, Springer-Verlag, New York, 1986.

Atreya, S. K., T. M. Donahue, and W. R. Kuhn, Evolution of a nitrogen atmosphere on Titan, *Science, 201*, 611–613, 1978.

Balla, R. J., K. H. Casleton, J. S. Adams, and L. Pasternack, Absolute rate constants for the reaction of CN with CH_4, C_2H_6 and C_3H_8 from 298 to 1500 K using high temperature photochemistry and diode laser asbsorption, *J. Phys. Chem., 95*, 8694–8701, 1991.

Banks, P. M., and G. Kockarts, *Aeronomy*, Academic, San Diego, Calif., 1973.

Barth, C. A., Nitric oxide in the lower thermosphere, *Planet. Space. Sci., 40*, 315–336, 1992.

Bézard, B., P. N. Romani, B. J. Conrath, and C. Maguire, Hydrocarbons in Neptune's stratosphere from Voyager infrared observations, *J. Geophys. Res., 96*, 18,961–18,975, 1991.

Bézard, B., A. Marten, and G. Paubert, First ground-based detection of cyanoacetylene on Titan, *Bull. Am. Astron. Soc., 24*, 953, 1992.

Bézard, B., A. Marten, and G. Paubert, Detection of acetonitrile on Titan, *Bull. Am. Astron. Soc., 25*, 1100, 1993.

Bruston, P., H. Poncet, F. Raulin, C. Cossart-Marcos, and R. Courtin, UV spectroscopy of Titan's atmosphere, planetary organic chemistry, and prebiological synthesis, I, Absorption spectra of gaseous propynenitrile ad 2-butynenitrile in the 185- to 250-nm region, *Icarus, 78*, 38–54, 1989.

Cabane, M., E. Chassefière, and G. Israel, Formation and growth of photochemical aerosols in Titan's atmosphere, *Icarus, 96*, 176–189, 1992.

Capone, L. A., J. Dubach, S. S. Prasad, and R. C. Whitten, Galactic cosmic rays and N_2 dissociation on Titan, *Icarus, 55*, 73–82, 1983.

Chamberlain, J. W., and D. M. Hunten, *Theory of Planetary Atmospheres*, Academic, San Diego, Calif., 1987.

Clarke, D. W., and J. P. Ferris, Photodissociation of cyanoacetylne: Application to the atmospheric chemistry of Titan, *Icarus, 115*, 119–126, 1995.

Connors, R. E., J. L. Roebber, and K. Weiss, Vacuum ultraviolet spectroscopy of cyanogen and cyanoacetylenes, *J. Chem. Phys., 60*, 5011–5024, 1974.

Courtin, R., D. Gautier, and C. P. McKay, Titan's thermal emission spectrum: Re-analysis of the Voyager infrared measurements, *Icarus, 114*, 144–163, 1995.

Coustenis, A., B. Bézard, and D. Gautier, Titan's atmosphere from Voyager infrared observations, I, The gas composition of Titan's equatorial region, *Icarus, 80*, 54–76, 1989.

Coustenis, A., B. Bézard, D. Gautier, and A. Marten, Titan's atmosphere from Voyager infrared observations, III, Vertical distributions of hydrocarbons and nitriles near Titan's north pole, *Icarus, 89*, 152–167, 1991.

Coustenis, A., T. Encrenaz, B. Bézard, G. Bjoraker, G. Graner, M. Dang-Nhu, and E. Arie, Modelling Titan's thermal infrared spectrum for high-resolution space observations, *Icarus, 102*, 240–260, 1993.

Crovisier, J., N. Biver, D. Bockelee-Morvan, P. Colom, L. Jorda, E. Lellouch, G. Paubert, and D. Despois, Carbon monoxide outgassing from comet P/Schwassmann-Wachmann 1, *Icarus, 115*, 213–216, 1995.

De More, W. B., and M. Patapoff, Temperature and pressure dependence of CO_2 extinction coefficients, *J. Geophys. Res., 77*, 6291–6293, 1972.

De More, W. B., J. J. Margitan, M. J. Molina, R. T. Watson, D. H. Golden, R. F. Hampson, M. J. Kurylo, C. J. Howard, and A. R. Ravishankara, Chemical kinetics and photochemical data for use in stratospheric modelling, Evaluation no. 7, *JPL Publ., 85-37*, 217 pp., 1985.

De More, W. B., M. J. Molina, S. P. Sander, D. M. Golden, R. F. Hampson, M. J. Kurylo, C. J. Howard, and A. R. Ravishankara, Chemical kinetics and photochemical data for use in stratospheric modelling, Evaluation no. 8, *JPL Publ., 87-41*, 196 pp., 1987.

Dubouloz, N., F. Raulin, E. Lellouch, and D. Gautier, Titan's hypothesized ocean properties: The influence of surface temperature and atmospheric composition uncertainties, *Icarus, 82*, 81–94, 1989.

English, M., L. M. Lara, R. D. Lorenz, P. M. Ratcliff, and R. Rodrigo, Ablation and chemistry of meteoric materials in the atmosphere of Titan, *Adv. Space Res., 17*, 157–160, 1996.

Frère, C., R. Raulin, G. Israel, and M. Cabane, Microphysical modelling of Titan's aerosols: Application to the in situ analysis, *Adv. Space Res., 10*, 159–163, 1990.

Glicker, S., and H. Okabe, Photochemistry of diacetylene, *J. Chem. Phys., 91*, 437–440, 1987.

Gurwell, M. A., and D. O. Muhleman, CO on Titan: Evidence for a well-mixed vertical profile, *Icarus, 117*, 375–382, 1995.

Hamai, S., and F. Hirayama, Fluorescence of acetylenic hydrocarbons, *J. Chem. Phys., 71*, 2934–2939, 1979.

Hanel, R., et al., Infrared observations of the Saturnian system from Voyager 1, *Science, 212*, 192–200, 1981.

Hidayat, T., A. Marten, B. Bézard, D. Gautier, T. Owen, H. E. Matthews, and G. Paubert, Millimeter and submillimeter heterodyne observations of Titan: Retrieval of the vertical profile of HCN and CO, *Bull. Am. Astron. Soc., 27*, 1106, 1995.

Hunten, D. M. (Ed.), The Saturnian system, *NASA Conf. Publ., 2068*, 1978.

Koch, E. E., and M. Skibowski, Optical absorption of gaseous methane, ethane, propane and butane and reflection of solid methane and ethane in the vacuum UV, *Chem. Phys. Lett., 9*, 429–432, 1971.

Kunde, V. G., A. C. Aikin, R. A. Hanel, D. E. Jennings, W. C. Maguire, and R. E. Samuelson, C_4H_2, HC_3N and C_2N_2 in Titan's atmosphere, *Nature, 292*, 686–688, 1981.

Laufer, A. H., E. P. Gardner, T. L. Kwok, and Y. L. Yung, Computations and estimates of rate coefficients for hydrocarbon reactions of interest in the atmospheres of the outer solar system, *Icarus, 56*, 560–567, 1983.

Lee, L. C., CN ($A\ ^2\Pi$-$X\ ^2\Sigma^+$) and CN ($B\ ^2\Sigma^+$-$X^2\Sigma^+$) yields from HCN photodissociation, *J. Chem. Phys., 72*, 6414–6421, 1980.

Lellouch, E., and D. M. Hunten, Titan's atmosphere engineering model, ESA Space Science Departmente International Publication ESLAB, pp. 87–199, Eur. Space Agency, Paris, 1987.

Lellouch, E., A. Coustenis, D. Gautier, F. Raulin, N. Dubouloz, and C. Frère, Titan's atmosphere and hypothesized ocean: A reanalysis of the Voyager 1 radio-occultation and IRIS 7.7 μm data, *Icarus, 79*, 328–349, 1989.

Lellouch, E., P. N. Romani, and J. Rosenqvist, The vertical distribution

and origin of HCN in Neptune atmosphere, *Icarus*, *108*, 112–136, 1994.

Lewis, J. S., Satellites of the outer planets: Their physical and chemical nature, *Icarus*, *15*, 174–185, 1971.

Lunine, J. I., Surface-atmosphere interactions on Titan, paper presented at Solar System Ices, Toulouse, France, March 27–30, 1995.

Lunine, J. I., D. J. Stevenson, and Y. L. Yung, Ethane ocean on Titan, *Science*, *222*, 1229–1230, 1983.

Lutz, B. L., C. de Bergh, and T. Owen, Titan: Discovery of carbon monoxide in its atmosphere, *Science*, *220*, 1374–1375, 1983.

Maguire, W. C., R. A. Hanel, D. E. Jennings, V. G. Kunde, and R. E. Samuelson, C_3H_8 and C_3H_4 in Titan's atmosphere, *Nature*, *292*, 683–686, 1981.

Marston, G., and L. J. Stief, Structure, spectroscopy and kinetics of the methylene amidogen (H_2CN) radical, *Res. Chem. Intermed.*, *12*, 161–186, 1989.

Marston, G., F. L. Nesbitt, and L. J. Stief, Branching ratios in the N + CH_3 reaction: Formation of methylene amidogen (H_2CN) radical, *J. Phys. Chem.*, *91*, 3483–3491, 1989a.

Marston, G., F. L. Nesbitt, D. F. Nava, W. A. Payne, and L. J. Stief, Temperature dependence of the reaction of nitrogen atoms with methyl radicals, *J. Phys. Chem.*, *93*, 5769–5774, 1989b.

Marten, A., D. Gautier, L. Tanguy, A. Lecacheux, C. Rosolen, and G. Paubert, Abundance of carbon monoxide in the stratosphere of Titan from millimeter heterodyne observations, *Icarus*, *76*, 558–562, 1988.

McKay, C. P., Elemental composition, solubility, and optical properties of Titan's organic haze, *Planet. Space. Sci.*, in press, 1996.

McKay, C. P., J. B. Pollack, and R. Courtin, The thermal structure of Titan's atmosphere, *Icarus*, *80*, 23–53, 1989.

Monks, P. S., P. N. Romani, F. L. Nesbitt, M. Scanlon, and L. J. Stief, The kinetics formation of nitrile compounds in the atmospheres of Titan and Neptune, *J. Geophys. Res.*, *98*, 17,115–17,123, 1993.

Mordaunt, D. H., I. R. Lamber, G. P. Morley, M. N. R. Ashfold, R. N. Dixon, C. M. Western, L. Schneider, and K. H. Welge, Primary product channels in the photodissociation of methane at 121.6 nm, *J. Chem. Phys.*, *98*, 2054–2065, 1993.

Moses, J. I., M. Allen, and Y. L. Yung, Neptune's visual albedo variations over a solar cycle: A pre-Voyager look at ion-induced nucleation and cloud formation in Neptune's troposphere, *Geophys. Res. Lett.*, *16*, 1489–1492, 1989.

Moses, J. I., M. Allen, and Y. L. Yung, Hydrocarbon nucleation and aerosol formation in Neptune's atmosphere, *Icarus*, *99*, 318–346, 1992.

Mount, G. H., and G. J. Rottman, The solar absolute spectral irradiance 1150–3173 Å: May 17, 1982, *J. Geophys. Res.*, *88*, 5403–5410, 1983.

Muhleman, D. O., G. L. Berge, and R. T. Clancy, Microwave measurements of carbon monoxide on Titan, *Science*, *223*, 393–396, 1984.

Nakayama, T., and K. Watanabe, Absorption and photoionization coefficients of acetylene, propyne and 1-butyne, *J. Chem. Phys.*, *40*, 558–561, 1964.

Nesbitt, F. L., G. Marston, and L. J. Stief, Kinetics studies of the reactions of H_2CN and D_2CN radicals with N and H, *J. Phys. Chem.*, *94*, 4946–4951, 1990.

Nesbitt, F. L., G. Marston, L. J. Stieff, M. A. Wickramaartchi, W. Tao, and R. B. Klem, Measurement of the photoionization spectra and ionization thresholds of the H_2CN and D_2CN radical, *J. Phys. Chem.*, *95*, 7613–7617, 1991.

Nesbitt, F. L., W. A. Payne, L. J. Stief, W. Tao, W.-H. Kuo, and R. B. Klemm, Quantitative determination of the rate and products of the reaction N + C_2H_5: The role of this reaction in the formation of HCN in the atmospheres of Titan and Neptune, paper presented at the Fourth International Conference on Laboratory Research for Planetary Atmospheres, Munich, 1992.

Nicolet, M., The photodissociation of water vapor in the mesosphere, *J. Geophys. Res.*, *86*, 5203–5208, 1981.

Nicolet, M., Photodissociation of molecular oxygen in the terrestrial atmosphere: Simplified numerical relations for the spectral range of the Schumann-Runge bands, *J. Geophys. Res.*, *89*, 2573–2582, 1984.

Nuth, J. A., and S. Glicker, The vacuum ultraviolet spectra of HCN, C_2N_2 and CH_3CN, *J. Quant. Spectrosc. Radiat. Transfer*, *28*, 223–231, 1982.

Okabe, H., Photochemistry of acetylene at 1470 Å, *J. Chem. Phys.*, *75*, 2772–2778, 1981.

Okabe, H., Photochemistry of acetylene at 1849 Å, *J. Chem. Phys.*, *78*, 1312–1317, 1983.

Paubert, G., D. Gautier, and R. Courtin, The millimeter spectrum of Titan: Detectability of HCN, HC_3N and CH_3CN and the CO abundance, *Icarus*, *60*, 599–612, 1984.

Pinto, J. P., G. R. Gladstone, and Y. L. Yung, Photochemical production of formaldehyde in the Earth's primitive atmosphere, *Science*, *210*, 183–184, 1980.

Podolak, M., and E. Podolak, A numerical study of aerosol growth in Titan's atmosphere, *Icarus*, *43*, 73–84, 1980.

Podolak, M., A. Bar-Nun, N. Tvoy, and L. P. Giver, Inhomogeneous models of Titan's aerosol distribution, *Icarus*, *57*, 72–82, 1984.

Pruppacher, H. R., and J. D. Klett, *Microphysics of Clouds and Precipitation*, D. Reidel, Norwell, Mass., 1980.

Rages, K., and J. B. Pollack, Titan aerosols: Optical properties and vertical distribution, *Icarus*, *41*, 119–130, 1980.

Rages, K., and J. B. Pollack, Vertical distribution of scattering hazes in Titan's upper atmosphere, *Icarus*, *55*, 50–62, 1983.

Rages, K., J. B. Pollack, and P. H. Smith, Size estimates of Titan's aerosols based on Voyager high-phase-angle images, *J. Geophys. Res.*, *88*, 8721–8728, 1983.

Raulin, F., Organic chemistry in the oceans of Titan, *Adv. Space Res.*, *7*, 71–81, 1987.

Reid, R. C., J. M. Prausnitz, and B. E. Poling, *The Properties of Gases and Liquids*, 4th ed., McGraw-Hill, New York, 1988.

Rodrigo, R., E. García-Alvarez, M. J. López-González, and J. J. López-Moreno, A nonsteady one-dimensional theoretical model of Mars' neutral atmospheric composition between 30 and 200 km, *J. Geophys. Res.*, *95*, 14,795–14,810, 1990.

Romani, P. N., A. Coustenis, E. Chassefiére, D. Toublanc, and L. M. Lara, Numerical modelling of Titan's photochemistry, *Bull. Am. Astron. Soc.*, *20*, 1087, 1990.

Romani, P. N., J. Bishop, B. Bézard, and S. Atreya, Methane photochemistry on Neptune: Ethane and acetylene mixing ratios and haze production, *Icarus*, *106*, 442–463, 1993.

Sagan, C., and W. R. Thompson, Production and condensation of organic gases in the atmosphere of Titan, *Icarus*, *59*, 133–161, 1984.

Samuelson, R. E., Ices in the atmospheres of various planets, paper presented at Solar System Ices, Toulouse, France, March 27–30, 1995.

Samuelson, R. E., and L. A. Mayo, Thermal infrared properties of Titan's stratospheric aerosol, *Icarus*, *91*, 207–219, 1991.

Samuelson, R. E., W. C. Maguire, R. A. Hanel, V. G. Kunde, D. E. Jennings, Y. L. Yung, and A. C. Aikin, CO_2 on Titan, *J. Geophys. Res.*, *88*, 8709–8715, 1983.

Sandford, S. A., and L. J. Allamandola, The condensation and vaporization behavior of H_2O:CO ices and implications for interstellar grains and cometary activity, *Icarus*, *76*, 201–224, 1988.

Shemansky, D. E., CO_2 extinction coefficient 1700–300 Å, *J. Chem. Phys.*, *56*, 1582–1587, 1972.

Slagle, I. R., D. Gutman, J. W. Davies, and M. Pilling, Study of the recombination reaction $CH_3 + CH_3 \rightarrow C_2H_6$, I, Experiment, *J. Phys. Chem.*, *92*, 2455–2462, 1988.

Smith, G. R., D. F. Strobel, A. L. Broadfoot, B. R. Sandel, D. E. Shemansky, and J. B. Holberg, Titan's upper atmosphere: Composition and temperature from the EUV solar occultation results, *J. Geophys. Res.*, *87*, 1351–1359, 1982.

Smyth, W. H., Titan's hydrogen torus, *Astrophys. J.*, *246*, 344–353, 1981.

Steiner, G., and S. J. Bauer, Molecular and eddy diffusion in the atmosphere of Titan, *Ann. Geophys.*, *8*, 473–476, 1990.

Strobel, D. F., The photochemistry of hydrocarbons in the atmosphere of Titan, *Icarus*, *21*, 466–470, 1974.

Strobel, D. F., Chemistry and evolution of Titan's atmosphere, *Planet. Space. Sci.*, *30*, 839–848, 1982.

Strobel, D. F., M. E. Summers, and X. Zhu, Titan's upper atmosphere: Structure and ultraviolet emissions, *Icarus*, *100*, 512–526, 1992.

Sun, Q., D. L. Yang, N. S. Wang, J. M. Bowman, and M. C. Lin, Experimental and reduced dimensionally quantum rate coefficients for $H_2(D_2)$ + CN → H(D)CN + H(D), *J. Chem. Phys.*, *93*, 4730–4739, 1990.

Tanguy, L., B. Bézard, A. Marten, D. Gautier, E. Gerard, G. Paubert, and A. Lecacheux, Stratospheric profiles of HCN on Titan from millimeter observations, *Icarus*, *85*, 43–57, 1990.

Thompson, W. R., and C. Sagan, Plasma discharge in N_2 + CH_4 at low

pressures: Experimental results and applications to Titan, *Icarus*, *90*, 57–73, 1991.

Toon, O. B., C. P. McKay, R. Courtin, and T. Ackerman, Methane rain on Titan, *Icarus*, *75*, 255–284, 1988.

Toon, O. B., C. P. McKay, C. A. Griffith, and R. P. Turco, A physical model of Titan's aerosols, *Icarus*, *95*, 24–53, 1992.

Toublanc, D., J. P. Parisot, J. Brillet, D. Gautier, F. Raulin, and C. P. McKay, Photochemical modeling of Titan's atmosphere, *Icarus*, *113*, 2–16, 1995.

Tsai, C., and D. L. McFadden, Gas phase atom-radical kinetics of atomic hydrogen, nitrogen and oxygen reactions with CHF radicals, *J. Phys. Chem.*, *94*, 3298–3300, 1990.

Weast, R. C., M. J. Astle, and W. H. Beyer, *Handbook of Chemistry and Physics 68th*, CRC Press, Boca Raton, Fla., 1987–1988.

West, G. A., and J. M. Berry, CN photodissociation and predissociation chemical lasers: Molecular electronic and vibrational laser emissions, *J. Chem. Phys.*, *16*, 4700–4716, 1974.

Yang, D. L., T. Yu, N. S. Wang, and M. C. Lin, CN radical reactions with selected olefins in the temperature range 174–740 K, *J. Chem. Phys.*, *160*, 317–325, 1992.

Yelle, R. V., Non-LTE models of Titan's upper atmosphere, *Astrophys. J.*, *383*, 380–400, 1991.

Yelle, R. V., D. F. Strobel, E. Lellouch, and D. Gautier, Recommended model for Titan's atmosphere, Eur. Space Agency Publ., in press, 1996.

Yung, Y. L., An update of nitrile photochemistry on Titan, *Icarus*, *72*, 468–472, 1987.

Yung, Y. L., and D. F. Strobel, Hydrocarbon photochemistry and Ly-α albedo at Jupiter, *Astrophys. J.*, *239*, 395–402, 1980.

Yung, Y. L., M. Allen, and J. P. Pinto, Photochemistry of the atmosphere of Titan: Comparison between model and observations, *Astrophys. J.*, *55*, 465–506, 1984.

Zelikoff, M., and K. Watanabe, Absorption coefficients of ethylene in the vacuum ultraviolet, *J. Opt. Soc. Am.*, *43*, 756–759, 1953.

L. M. Lara and E. Lellouch, DESPA, Observatoire de Paris-Meudon, 92195 Meudon Cedex, France.

J. J. López-Moreno and R. Rodrigo, Instituto de Astrofísica de Andalucía CSIC, Apdo. 3004, 18080 Granada, Spain.

(Received August 7, 1995; revised June 21, 1996; accepted June 28, 1996.)